REVIEW

Recent Progress of Graphene Fiber/Fabric Supercapacitors: From Building Block Architecture, Fiber Assembly, and Fabric Construction to Wearable Applications

Tuxiang Guan[1] · Zemei Li[1] · Dianchun Qiu[1] · Guan Wu[2] · Jian Wu[1] · Liping Zhu[3] · Meifang Zhu[3] · Ningzhong Bao[1]

Abstract

High-performance fiber-shaped power sources are anticipated to considerably contribute to the continuous development of smart wearable devices. As one-/two-dimensional (1D/2D) frameworks constructed from graphene sheets, graphene fibers and fabrics inherit the merits of graphene, including its lightweight nature, high electrical conductivity, and exceptional mechanical strength. The as-fabricated graphene fiber/fabric flexible supercapacitor (FSC) is, therefore, regarded as a promising candidate for next-generation wearable energy storage devices owing to its high energy/power density, adequate safety, satisfactory flexibility, and extended cycle life. The gap between practical applications and experimental demonstrations of FSC is drastically reduced as a result of technological advancements. To this end, herein, recent advancements of FSCs in fiber element regulation, fiber/fabric construction, and practical applications are methodically reviewed and a forecast of their growth is presented.

Keywords Graphene fibers/fabrics · Flexible supercapacitor · Element regulation · Fiber/fabric construction · Wearable application

Introduction

The expansion of wearable electronic device has altered the present standards for energy storage devices and prompted substantial research on next-generation power sources [1, 2]. Due to its greater flexibility, wearability, cycling stability, and high energy/power density, FSCs have garnered considerable attention in this area [3]. As electrode materials, several flexible fiber materials, such as metal wire [4], carbon fiber [5], cotton fiber [6], and MXene [7], have been utilized to date. Correspondingly, fabricated FSCs demonstrate biodegradability [8], self-healing [9], and self-powered [10], which broaden the industrial uses of fiber-shaped power sources. Although significant progress has been made, fiber electrodes still suffer from poor structural processability, low conductivity, and low specific surface area (SSA), resulting in straggling ion diffusion and storage as well as electron transmission.

Owing to its two-dimensional lamellar structure, satisfactory dispersibility/processability, and high industrial output, graphene and its derivatives have been extensively studied as flexible fiber electrodes in recent years [11]. The constructed graphene fiber/fabric demonstrates high conductivity, high SSA, outstanding mechanical stability, and low weight, making it a great choice for flexible electrodes in FSCs [12, 13]. In addition, due to the high dispersibility and processability of graphene oxide (GO) in a variety of solvents, graphene fibers/fabrics can be easily manufactured by altering external stress distribution, temperature fluctuation, and chemical components. Correspondingly, the high diversity in fiber preparation methods provides multiple approaches to adjust

✉ Ningzhong Bao
nzhbao@njtech.edu.cn

1 State Key Laboratory of Materials-Oriented Chemical Engineering, College of Chemical Engineering, Nanjing Tech University, Nanjing 210009, People's Republic of China

2 National Engineering Lab for Textile Fiber Materials and Processing Technology, School of Materials Science and Engineering, Zhejiang Sci-Tech University, Hangzhou 310018, People's Republic of China

3 State Key Laboratory for Modification of Chemical Fibers and Polymer Materials, College of Materials Science and Engineering, Donghua University, Shanghai 201620, People's Republic of China

the physical structure of fibers/fabrics on a micro–macro scale. Thus, based on the distinct fabrication technique, the as-designed fiber possesses the distinguishing characteristics of high mechanical strength, good conductivity, and satisfactory electrochemical activity. A high-temperature enclosed environment is effective for removing oxygen-containing groups from GO. Under the confinement effect of the van der Waals force, the resulting reduced GO (rGO) sheets self-assemble into fibers. In addition, under the strong shear force action of the spinneret channel, GO prefers to arrange itself in an orderly fashion in the wet-spinning method. Correspondingly, the graphitized graphene fiber possesses a strength of 2.4 GPa and an electrical conductivity of 3.5×10^5 S/m [14]. In addition, pseudocapacitive materials, such as oxides [15], sulfides [16], metal–organic frameworks [17], and conductive polymers [18], are induced in the graphene fibers to further improve the electrochemical activity of composite fibers. Moreover, graphene fiber fabric can be further obtained through orienting or randomly arranging fibers [19, 20]. This kind of novel carbon fabric with a single graphene fiber as the basic component not only inherits the good flexibility of graphene fiber, but also has good integration and energy output capability. In this regard, graphene fiber-based fiber and fabric supercapacitors both constitute a promising flexible energy source for wearable electronic device.

Several outstanding reviews have summarized the rapid development of graphene fibers/fabrics to date. For example, Gao et al. [21] provided a comprehensive overview of the synthesis, morphology, structure-performance correlations, and advanced applications of graphene fibers. Another significant study by Qu et al. [22] provided a comprehensive review of the preparation techniques, performance enhancement strategies, and novel application of graphene fibers. However, from the perspective of the fiber/fabric preparation process, it is still necessary to understand the effect of fiber components and fiber structure on the performance of flexible devices. Herein, the fiber/fabric preparation process is primarily divided into three steps: (1) the regulation of fiber constituents (such as GO), (2) assembly of fibers, and (3) production of fabrics [23]. In this context, the correlation between the elements and the fibers/fabrics are examined to determine their effect on the electrochemical/mechanical performance of flexible fiber/fabric supercapacitors. As shown in Fig. 1, the impacts of various regulation strategies on the properties of fiber elements are discussed, including heteroatomic doping, reduction, and defect reparation. Then, the preparation methods of graphene fiber are summarized to analysis the origin of diverse fiber shapes, which are crucial to the overall performance of fiber electrodes. Subsequently, the approaches for integrating graphene fibers into
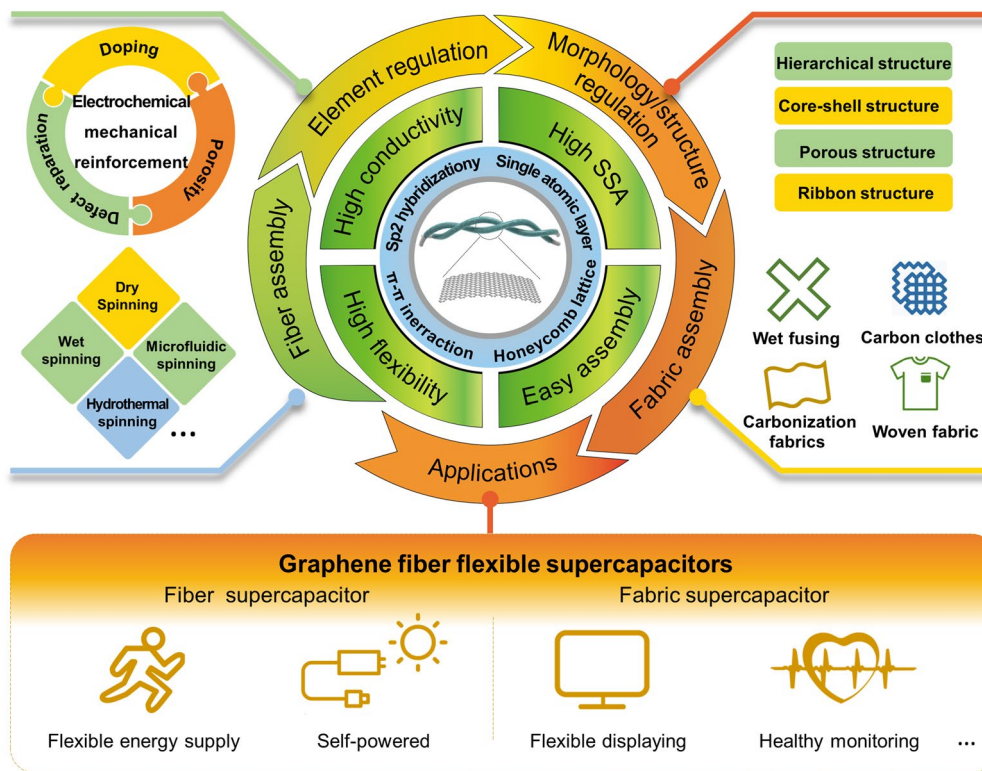

Fig. 1 The illustration of chemical fabrication and regulation of graphene fiber supercapacitors

fabrics and flexible supercapacitors are reviewed, which highlights the flexible energy storage strategy for future smart portal devices.

Energy Storage Mechanism of Fiber/Fabric Supercapacitor and Preparation of GO/Graphene

Energy Storage Mechanism of Fiber/Fabric Electrode

Double-Layer Capacitance

Generally, fiber/fabric supercapacitors consist of two flexible electrodes, sandwiching a solid electrolyte. The flexible electrode functions as the collector and active materials of the electrode. As seen in Fig. 2a, the charging and discharging mechanisms of fiber/fabric flexible supercapacitors can be categorized into three groups: (1) electrochemical double-layer capacitor (EDLC), which is characterized by the reversible electrostatic adsorption of electrolyte ions on carbon materials with high SSA; (2) pseudocapacitance, the storage of charge by fast interfacial redox reactions of electrochemically active materials; and (3) a hybrid capacitor consisting of EDLC and pseudocapacitance [24]. The electrified interface structure of an ELDC was first described by Helmholtz using Eq. (1).

$$C = \varepsilon_0 \varepsilon_r A/d, \tag{1}$$

where ε_0 is the vacuum dielectric constant, ε_r is the electrolyte dielectric constant, A is the electrode surface area, and d is the charge separation distance.

In the capacitance model improved by Gouy and Chapman as well as Stern and Geary, the diffusion layer of electrolyte ions was further considered for the capacitance model [25]. Simon et al. recently witnessed more precise charge separation behavior on polarization at the electrode–electrolyte interface [26]. As depicted in Fig. 2b, as the pore size decreases, the normalized capacitance decreases as a result of the compact ion layer on the pore walls, which reduces the surface area available for double-layer formation. Because the distortion of the solvation shells reduces the distance between the ion center and the electrode surface, further reduction of the pore size to less than the size of the solvated ion (< 1 nm) results in a significant increase in the normalized capacitance. Subsequent experiments validated this discovery. As illustrated in Fig. 2c, as the radius of the pore's curvature decreases, the contact between the ions and the carbon wall becomes stronger, leading to an increase in the amount of charge stored per carbon in the three-dimensional (3D) porous carbon nanopore [27].

However, the disparity between the values predicted by the theoretical model and actual experimental outcomes persists. As depicted in Fig. 2d, when the number of graphene layers is reduced to a single layer or a small number of layers, the capacitance is abnormally increased, comparable to that of a battery. This divergence in the experimental results of two-dimensional graphene may occur from the interaction between the p-band Fermi liquid and Helmholtz layers ions. Due to electrostatic shielding, an increase in the number of graphene layers gradually reduces capacitance [28]. Notably, due to the stronger π–π stacking effect of graphene, which may lower capacitance, multilayer graphene structures are more common in practical applications. Consequently, minimizing the restacking effect of graphene and increasing the number of ion transport pathways is a crucial method for enhancing the performance of graphene electrodes.

Pseudocapacitance

Pseudocapacitance relates to the fast Faraday reaction on the surface of pseudocapacitive materials that present fast charge storage rate. Its capacitance can be calculated using the following equation (Eq. (2)):

$$C = \frac{Q}{V} = \left(\frac{nF}{m}\right)\frac{X}{V}, \tag{2}$$

where X is the ion coverage range of the surface (or inner surface) of the active material, m is the molecular weight of the active material, n is the number of electrons, F is the Faraday constant, Q is the stored electric quantity, and V is the voltage [29]. Based on their reaction mechanisms, pseudocapacitance can be further divided into surface redox pseudocapacitance and intercalated pseudocapacitance. Intercalated pseudocapacitors primarily store ions via ionic conduction or fast ion diffusion inside the host material (such as Nb_2O_5, [30] and Mxene [31]). Charge is stored in surface redox materials through charge transfer on or near the surface [32] (such as MnO_2, [33] RuO_2, [34] and conductive polymers [35]). Typically, ion intercalation behaviors occur on the surface of materials, which is mostly unaffected by ionic diffusion; thus, the test current in CV curves increases linearly with increasing scanning rate. Equation (3) relates the reaction of the scanning current to the scanning rate.

$$i(v) = av^b, \tag{3}$$

where a is constant, b is power-law exponential. For the battery material controlled by the diffusion process, the b value is 0.5 [36]. For the EDLC, the b value is 1, and for pseudocapacitors, the b value is ~ 1 [36]. Thus, in the case of graphene fibers/fabrics compounded with pseudocapacitive materials, the total current contributed by the two capacitors can be calculated using the following equation (Eq. (4)):

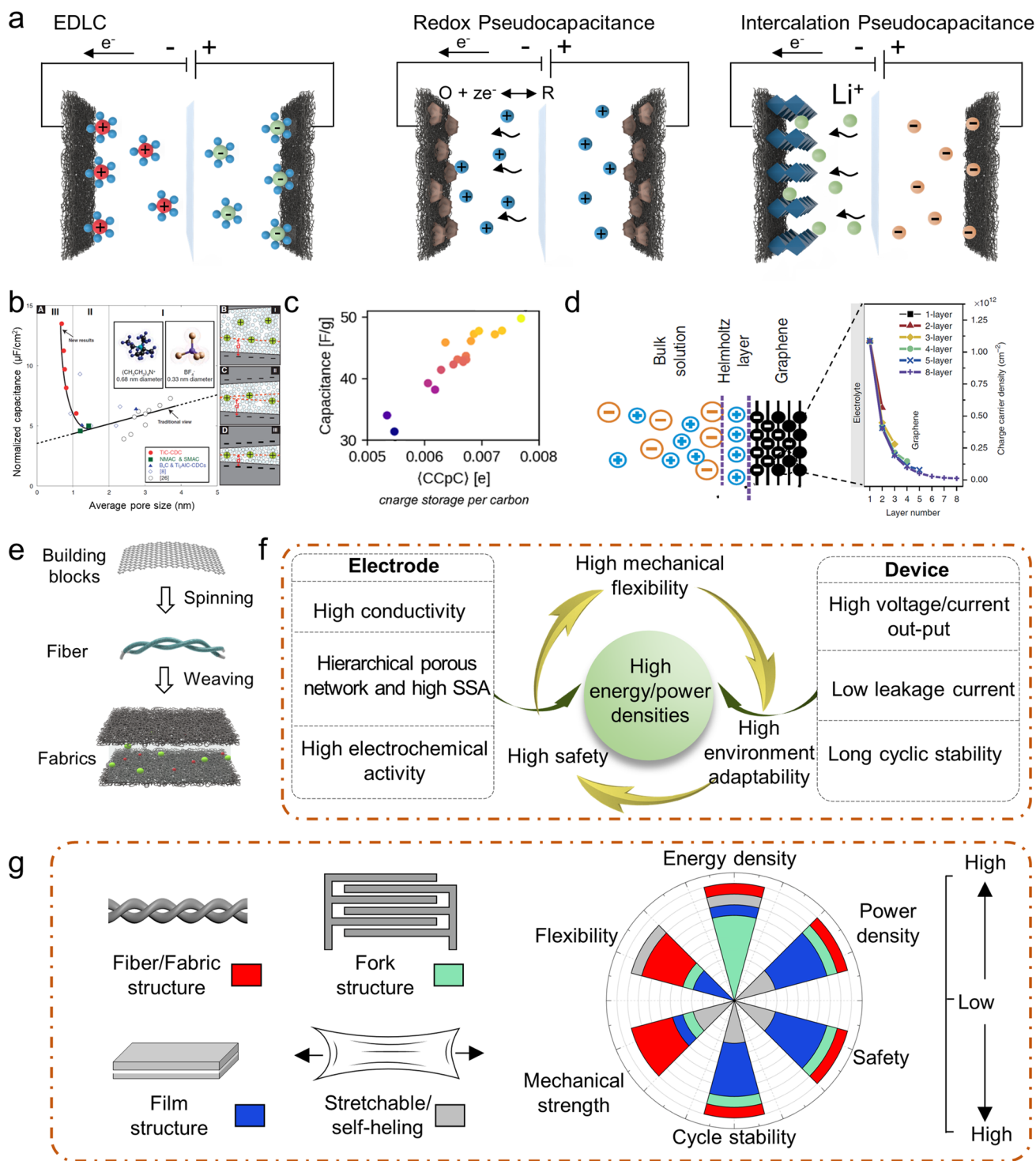$$i(v) = k_1 v + k_2 v^{1/2}, \tag{4}$$

Fig. 2 **a** Energy storage mechanism of supercapacitors. **b** The correlation between average pore size and normalized capacitance; reproduced with permission from Ref. [26], Copyright 2006, AAAS. **c** Charge storage per carbon under the different radii of curvature; reproduced with permission from Ref. [27], Copyright 2019, American Chemical Society (ACS). **d** Charge distribution in graphene electrodes with different numbers of layers; reproduced with permission from Ref. [28], Copyright 2014, Nature Publishing Group (NPG). **e** Schematic illustration of the construction process of fiber/fabric supercapacitors. **f** Factors affecting the performance of fiber/fabric supercapacitors

where $k_1 v$ is the current contributed by the capacitor process (including double-layer capacitance and interlayer pseudocapacitance) and $k_2 v^{1/2}$ is the current controlled by the solid-state diffusion control process. Subsequently, Eq. (4) may be transformed into Eq. (5) as follows:

$$\frac{i(V)}{v^{1/2}} = k_1 v^{1/2} + k_2. \tag{5}$$

By comparing $k_1 v^{1/2}$ with k_2, the radio contributed by surface process control can be calculated [37].

Hybrid Capacitor

Hybrid supercapacitor stores energy by comprising EDLC and redox materials. This design of different energy storage mechanisms of respective electrodes endows hybrid supercapacitor to presents both the features of high energy density and high-power density. To be specific, redox materials can improve the energy density, while EDLC materials can improve the power density [38]. Additionally, the operating voltage window can also be effectively expanded due to this asymmetric assembling of the positive and negative electrode materials. According to Eq. (6),

$$E = \frac{1}{2}CV^2, \tag{6}$$

where E is energy density, C is specific capacitance, V is voltage. The energy density is proportional to the square of voltage; therefore, the high working voltage of hybrid supercapacitor is conducive to achieve higher energy density. The potential window of a hybrid supercapacitor can be acquired by Eq. (7),

$$E = E_0 + \Delta E_1 + \Delta E_2 = \frac{1}{F(\omega^\beta - \omega^\alpha)N_A} + \Delta E_1 + \Delta E_2, \tag{7}$$

where ω^α and ω^β represents the work function of positive and negative electrode, N_A represents Avogadro's number, F represents 1 Faraday (96 485 C), ΔE_1 and ΔE_2 represents surface dipole potentials of the positive and negative electrodes [39]. On this point, in the progression towards high electrochemical performance hybrid capacitors, select and synthesize appropriate positive and negative electrode materials are prior to realize the promising potential of their synergistic effects.

The construction of FSC is depicted in Fig. 2e. First, the modified fiber pieces are assembled into 1D fibers through the spinning process. Then, the fiber is integrated as a 2D fabric electrode during the weaving process, which further improves the voltage and current output capacity and expands the application range of the fiber/fabric supercapacitor. According to the storage mechanism of

supercapacitors, as depicted in Fig. 2f, the following factors have a significant impact on electrochemical performance:

1. high electrical conductivity to promote rapid electron transfer;
2. high SSA porous structure and to provide abundant ion adsorption sites;
3. high electrochemical activity to provide stronger charge storage capacity.

At the device level, features including high output voltage, low leakage current, and long cycle life are highly desired. In level of industrial design and fabrication, high mechanical flexibility, high security, and good environmental adaptability are also required to adapt to different application scenarios [40]. To further evaluate feature and priority of FSC, the electrochemical and mechanical performance of different flexible supercapacitors were compared from perspectives of energy density, power density, safety, cycle stability, mechanical strength and flexibility. In principle, basing on the device structure and function, the flexible supercapacitors may be divided into four types: fiber/fabric structure, film structure, fork structure and high stretchable/self-heling structure. As is shown in Fig. 2g, benefitting from the 1D/2D assembled architectures, porous network, and adjustable preparation methods, fiber/fabric supercapacitors present priority in mechanical strength, flexibility, energy density and safety. It is also quite competitive in terms of power density and cycle stability. In this context, graphene fiber-based supercapacitor is an attractive candidate to the next-generation flexible energy storage device for wearable electronic system.

Preparation and Regulation of GO/Graphene

Preparation of GO/Graphene

Depending on the preparation process, graphene and its derivatives can be divided into three types: graphene nanosheets (non-oxidized), chemical prepared GO, and chemical vapor deposition (CVD) grown graphene film (Fig. 3a) [41]. Thereinto, chemically preparing GO through modified Hummers method presents the advantages of low cost, high yield, easy to perform, and safety, thus play a pivotal role in the industrial production of graphene fiber/fabric [42]. Graphite is typically oxidized using $KMnO_4$ as the oxidizing agent and sulfuric acid as the acidic medium, as depicted in Fig. 3b. The graphite oxide was then obtained by water washing [43]. Correspondingly, graphite oxide spontaneously exfoliates into a single-layer GO during the washing process, which can then be centrifuged into high-concentration monolayer GO. However, this approach produces a low yield of monolayer GO, resulting in the waste of raw materials.
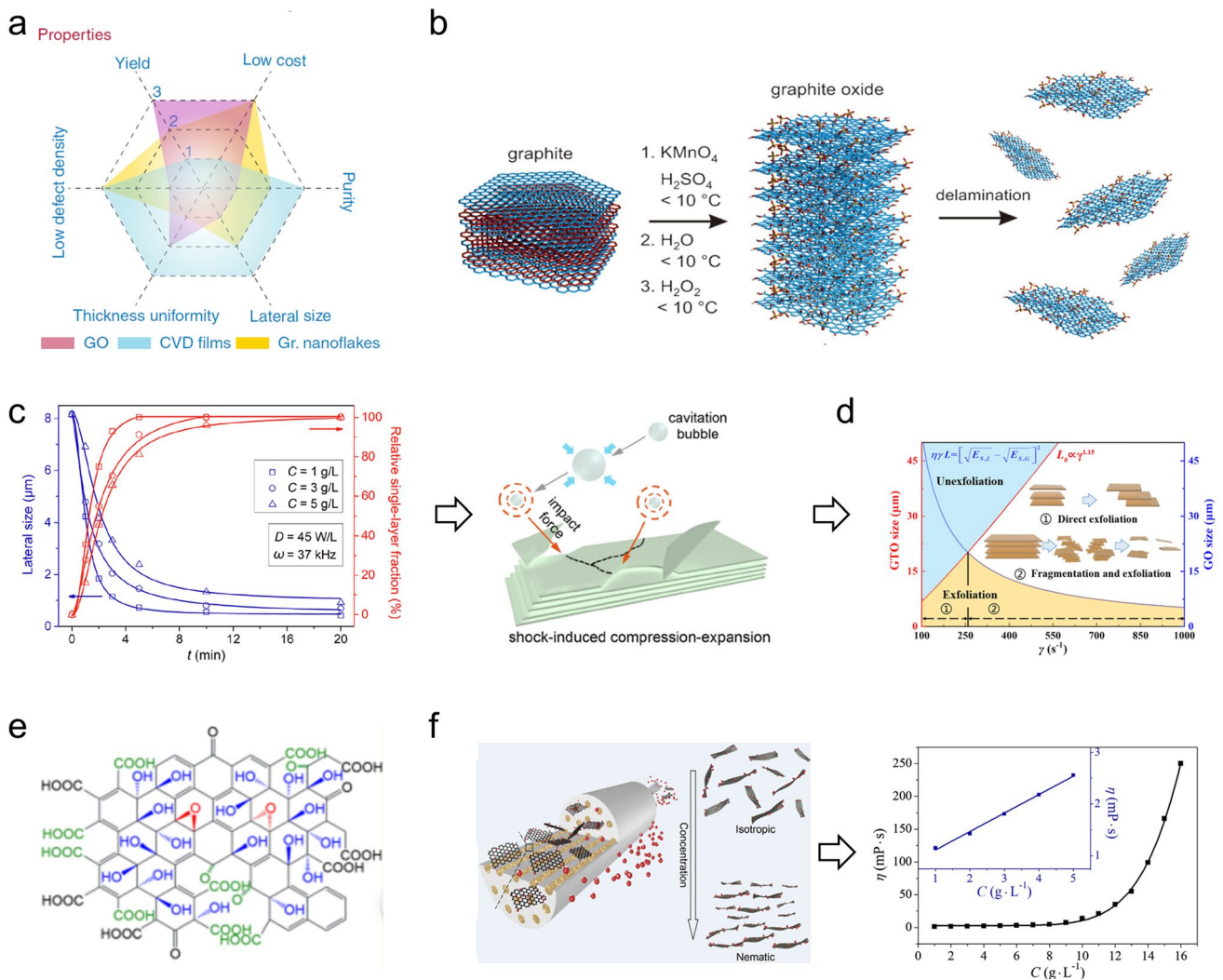
Fig. 3 Preparation and regulation of GO/graphene. **a** Comparison of the properties of different graphene products; reproduced with permission from Ref. [41], Copyright 2019, NPG. **b** Schematic illustration of the synthesis of GO; reproduced with permission from Ref. [43], Copyright 2014, Wiley. **c** Plots of lateral size and relative single-layer fraction against the exfoliation duration of exfoliated graphite oxide sheets (left) and ultrasound-assisted exfoliated mechanism of graphite oxide (right); reproduced with permission from Ref. [44], Copyright 2020, Elsevier. **d** Schematic illustration of the shear exfoliation process; reproduced with permission from Ref. [46], Copyright 2021, Springer. **e** Chemical structure of GO; reproduced with permission from Ref. [47], Copyright 2016, ACS. **f** Schematic illustration of the cross-flow filtration process of GO dispersions (left) and viscosity of GO aqueous dispersions in the concentration range of 1–16 g/L (right); reproduced with permission from Ref. [48], Copyright 2019, Elsevier

Additional exfoliation could enhance the final monolayer radio product. As shown in Fig. 3c, Bao et al. investigated the ultrasonic exfoliation process of graphite oxide by examining the viscosity change of graphite oxide during ultrasound [44]. Using ultrasound, graphite oxide can be completely exfoliated in several minutes with a virtually 100% yield, as evidenced by the drop in viscosity. However, it is impossible to control the impact effect of cavitation bubbles, resulting in the destruction of GO. Consequently, the size of monolayer GO produced by ultrasound-assisted exfoliation is small (<3 μm). This small lateral dimensions results in a high critical concentration of GO crystal and inhibit the improvement

of the mechanical characteristics of the graphene fibers [45]. To reduce the fragmentation and boost the yield of monolayer GO, a shear exfoliation technique is devised [46]. During the exfoliation procedure, the shear force can be precisely controlled by manipulating the rotational speed and form of the propeller. Accordingly, the experimental results demonstrate that fragmentation is well prevented during the shear exfoliation process, resulting in an average lateral size of 14 μm with an 80% monolayer ratio (Fig. 3d).

The chemical structure of GO is depicted schematically in Fig. 3e, with carboxyl groups at the edge and hydroxyl and epoxy groups in the plane. These polar functional groups can

ionize protons in water and negatively charge GO accounting for the good dispersity of GO [47]. Following washing and exfoliation, the concentration of GO dispersion is typically low, whereas a high concentration of the spinning solution is required for the spinning of graphene fibers. Traditional concentration techniques, such as rotary evaporation and centrifugation, are plagued by excessive energy consumption and the simple stacking of GO throughout the concentration process. To address this issue, Li et al. created a cross-flow membrane filtration device and thoroughly studied the effects of membrane aperture and operating parameters (transmembrane pressure difference and tangential flow rate) on the filtering efficiency (Fig. 3f). With a maximum concentration of 16 g/L, GO dispersion is converted from a disordered condition to an anisotropic liquid crystal phase during cross-flow membrane filtration [48].

Reduction of GO

Despite the oxygen-containing functional groups that provide GO with good dispersibility and processability in water, the honeycomb structure of graphene is disrupted, resulting in low electrical conductivity. Consequently, oxygen-containing functional groups must be eliminated to restore the sp^2 hybridization of the carbon skeleton. In this regard, chemical reduction comprises one of the most efficient strategies for GO reduction. The resultant reduced graphene oxide sheet is normally clarified as rGO. Correspondingly, hydrazine hydrate has been the most commonly utilized reducing agent, and its reduction mechanism has been extensively studied. In the reduction process, hydrazine combines with the epoxy group on GO to create hydrazol and amino-nitrogen heterocycles, which are capable of forming carbon–carbon double bonds through the thermal elimination of di-imide [49]. Ren et al. hypothesized that the carboxyl group on GO may react with hydrazine to generate a hydrazone-type bond (–C=N–N=C–) [50]. However, Cheng et al. discovered that immersing GO films in a strong reducing agent such as hydrazine hydrate generates many bubbles, destroying the structure of GO assemblies [51]. In contrast, HI is a more appropriate reducing agent. When submerged in HI solution, the GO film is rapidly degraded while retaining its structure. Gao et al. further compared the reduction effects of hydrazine hydrate and HI. To prevent the fibers from being crushed, the GO fibers were reduced by hydrazine hydrate steam. The results indicate that graphene fibers reduced by hydrazine hydrate have a relatively loose structure, whereas the HI reduced fibers present a more compact structure and superior electrochemical performance owing to their higher electrical conductivity [52].

Thermal reduction is an additional efficient way for GO reduction. Correspondingly, the content of the oxygen-containing functional group can be easily adjusted by controlling the reduction temperature and time. When the ambient temperature hits 300 °C, the oxygen-containing functional groups on GO begin to degrade significantly, releasing H_2O, CO_2, and CO [53]. As the temperature increases, the oxygen-containing functional groups breakdown slowly, producing graphene sheets with a greater reduction extent. Another adjustable component in functional group adjustments is the reduced environment external. According to previous studies, the de-oxidation activation energy of GO in vacuum is ~ 155 kJ/mol (1.6 eV/atom) [53]. Under hydrothermal conditions with water as the medium, the deoxygenation reaction will be accelerated, resulting in a 95 °C drop in deoxygenation temperature [54]. In contrast, at the same temperature, the deoxygenation reaction reacts much more slowly in vacuum and at normal pressure.

Preparation of Graphene Fiber

Prepare Graphene Fiber by Wet-Spinning Method

Wet-spinning is one of the most promising techniques for producing graphene fibers due to its simplicity, operability, and large-scale production ability. According to the Onsager LC theory, the GO solution will transition to the liquid crystal phase when its concentration exceeds the critical concentration (φ), which is determined by the aspect ratio of GO sheets. Under the influence of shear force, the GO sheets will arrange themselves in an orderly fashion along the direction of the force to create the basal structure of graphene oxide fibers (Fig. 4a I) [55]. Finally, after drying and reduction, graphene fibers are obtained (Fig. 4a II) [21]. This continuous spinning process is affected by numerous parameters, including solution concentration, spinning solution solvent, the physical/chemical properties of GO, spinneret geometrical parameters, solidification bath, spinning temperature, and coagulation time [56]. Consequently, solution concentration comprises one of the critical factors. Compared with the high-concentration GO solution, a decrease in the GO concentration will encourage the orderly arrangement of GO, resulting in a fiber with greater mechanical strength [57]. Additional research reveals that the fluctuation of the shear force domain is associated with this process. Under conditions of relatively high shear rate, GO solutions tend to generate Taylor vortices that disrupt the orderly arrangement of GO. The relationship between the alignment extent of GO and shear rate is nonlinear, and at the ideal shear threshold, the mechanical characteristics of graphene fibers can be enhanced by 54% [58].

The selection of suitable coagulation bath is a crucial stage in the spinning process. The negative charge on the surface of GO dictates its solubility in an aqueous solution (known as ζ potential). A lower ζ potential suggests an increase in negative charge on the surface of GO, resulting in
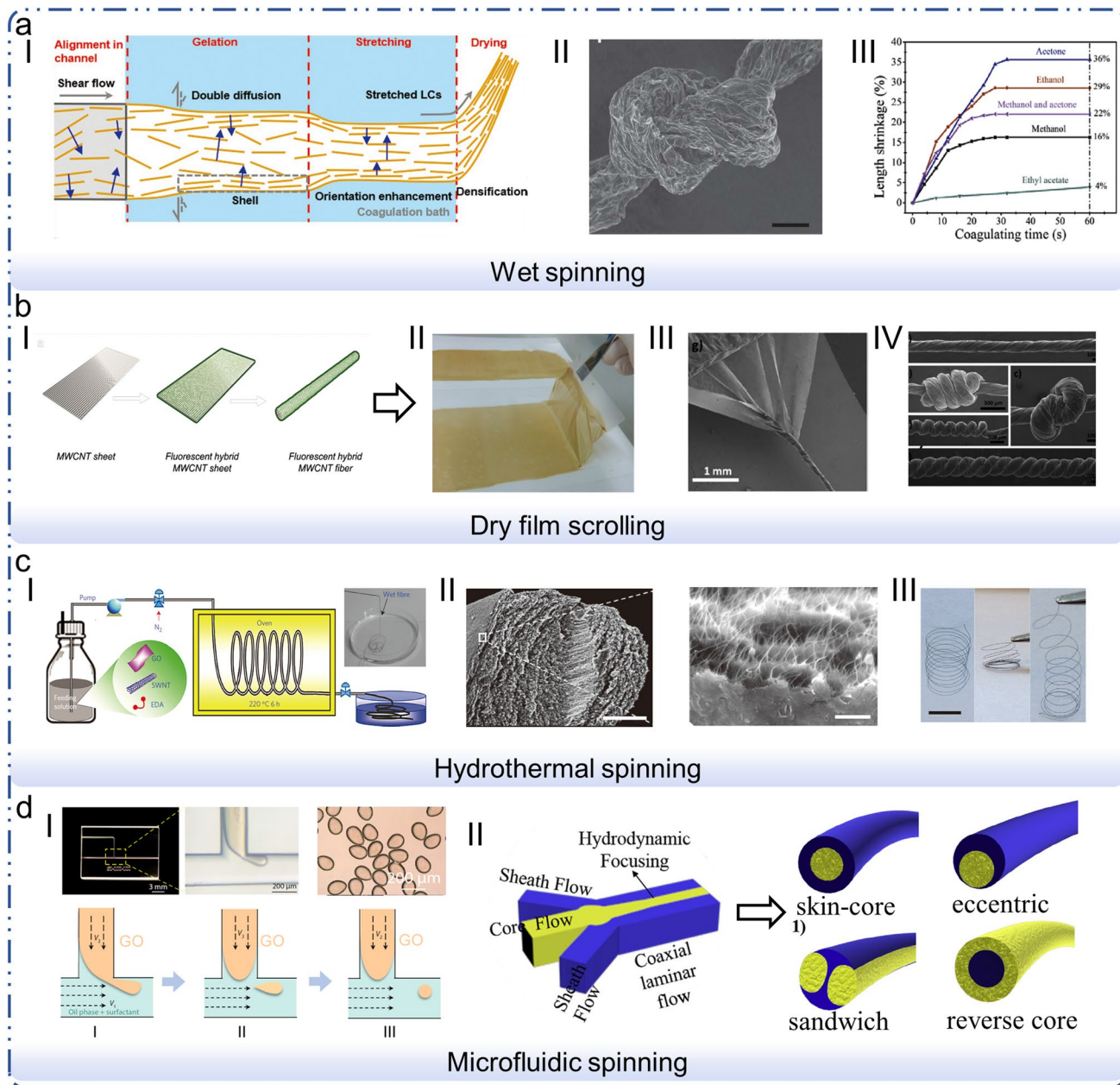
Fig. 4 Methods for the preparation of graphene fibers. **a** Wet-spinning of graphene fiber: I. the spinning mechanism; reproduced with permission from Ref. [21], Copyright 2020, Wiley; II. SEM image of graphene fiber; reproduced with permission from Ref. [55], Copyright 2011, NPG; III. The length shrinkage of GO fiber against coagulating time under different coagulation baths; reproduced with permission from Ref. [60], Copyright 2018, Elsevier. **b** Dry film scrolling of graphene fiber: I. Schematic illustration of the preparation procedures of the CNT fiber electrode; reproduced with permission from Ref. [62], Copyright 2018, Wiley; II. Free-standing thin GO film; III. SEM image of thin GO film; IV. SEM images of GO fibers with different morphologies and knot architectures; reproduced with permission from Ref. [63], Copyright 2014, ACS. **c** Hydrothermal-spinning of graphene fiber: I. Schematic of the fabrication of carbon hybrid microfibers; II. SEM images of the cross section of graphene/CNT fiber; III. Compressed and stretched fiber springs; reproduced with permission from Ref. [64], Copyright 2014, NPG. **d** Microfluidic-spinning of graphene fiber: I. GO liquid crystal microdroplets; reproduced with permission from Ref. [65], Copyright 2021, NPG; II. Schematic illustration of microfluidic-spinning process and four cases of structure-tunable bicomponent fibers (STBFs) with distinct cross-sectional shapes; reproduced with permission from Ref. [66], Copyright 2019, Elsevier

in enhanced dispersion. Injecting the GO solution into an appropriate coagulation bath destabilizes the GO solution and causes GO to coagulate into GO gel fibers. Based on the various types of coagulation bath, the coagulation process may be loosely categorized into three mechanisms: 1. cationic crosslinking; 2. GO deprotonation; and 3. GO partial reduction. For mechanism 1, salt solutions, such as CuCl$_2$ [57] cetyltrimethylammonium bromide (CTAB) solution [59], are often chosen as coagulation baths. These salt solutions include cations that crosslink with negatively charged GO, resulting in GO coagulation. For the second solidification mechanism, organic solvents such as ethanol [60], acetic acid, [15] acetone [61], are frequently acceptable. When GO is injected into these solutions, the negatively charged GO will be reprotonated, leading to the flocculation of GO under the influence of van der Waals forces. Due to the rapid solvent exchange rate, this form of coagulation bath has an exceptionally high coagulation rate and a short coagulation period of a few seconds, which facilitates the continuous commercial production of graphene fibers. However, such a strong solidification action will result in a significant shrinking of fibers during coagulation, deviating the fiber cross section from the circle (Fig. 4a III) [60]. In comparison to a circular cross section, this uneven cross section may produce a greater number of flaws, resulting in a decline in mechanical strength and stability. Inducing a reductant into the coagulation solution to partially reduce GO during spinning is the third mechanism of coagulation. It is frequently paired with the initial and secondary solidification mechanisms. Zhang et al., for instance, added a small amount of N$_2$H$_4$·H$_2$O to an ethanol solution to reduce GO throughout the solidification process. Under the influence of the van der Waals force, partially reduced GO will flocculate upon the recovery of the graphene carbon skeleton. The as-prepared nonwoven graphene fiber fabric showed good mechanical and electrochemical properties [20].

Preparation of Graphene Fibers Using the Dry-Spinning Method

Typically, in the case of the dry-spinning method, GO solution is immediately extruded through the spinneret, followed by the progressive evaporation of the solvent and the direct drying of the solution into GO fiber. In contrast to the wet-spinning method, only the drying process is required, which greatly simplifies the spinning procedure. Correspondingly, the selection of the right solvent to dissolve GO is a crucial step in dry-spinning.

Due to the surface tension of the solvent, the spinning solution tends to congregate around the spinneret and cannot form fibers after being squeezed from the spinneret. Tian et al. suggested that the optimal solvent should strike a balance between parameters such as the dispersity of GO,

volatile rate and expressive tension of the solvent [67]. Low surface tension can reduce the tendency of a liquid to condense into droplets, which is caused by the Rayleigh instability of a flowing solvent. In addition, the fast evaporation rate ensures the quick drying of GO fibers. Moreover, a high dispersion ensures that the spinning process and orderly arrangement of GO are performed smoothly. Correspondingly, the mixed solution of tetrahydrofuran and water exhibits the best spinning performance after screening. The produced graphene fiber exhibits a hardness of up to 19.12 MJm^{-3}, demonstrating the feasibility of dry-spinning. Increasing the concentration of GO spinning solution was another method to solve the accumulation of spinning solution at the spinneret. Chen et al. synthesized a GO solution with a high concentration by rotary evaporation [68]. As the concentration of GO solution increased, the fluidity of the spinning solution reduced until it was sufficiently viscous to sustain the fiber structure. The extruded GO gel fibers were transferred into high-temperature chambers, where they were dried and then converted to graphene fibers. Because of the weak shear action of high-concentration GO fiber in the extrusion process, the fiber orientation degree (OD) was low and the tensile strength was 127.5 MPa. In contrast, a remarkable elongation (13.5%) was achieved.

Preparation of Graphene Fibers Using the Thin Film Shrinkage Method

The thin film shrinkage method makes use of physical twisting to turn graphene film into graphene fibers; the resulting graphene fiber exhibits extraordinarily high elasticity and tensile strength. Initially, this process was used to prepare carbon nano tube (CNT) fibers. Peng et al. twisted the CNT slices removed from the CNT array, as illustrated in Fig. 4b I. Due to van der Waals forces, carbon nanotubes were interwoven and tightly linked throughout this procedure to generate CNT fibers. Due to the significant shear stress given to the GO film during twisting, a GO film with high tensile strength is necessary [62]. Correspondingly, Terrones et al. created GO films with a thickness of 0.74 μm using polytetrafluoroethylene (PTEE) as the substrate and large-sized GO as the precursor via the scratch coating technique (Fig. 4b II) [63]. Benefiting from the rough surface of the PTEE substrate and fewer edge flaws of the large-sized GO, the produced GO film exhibits outstanding mechanical flexibility to ensure the success of the twisted technique (Fig. 4b III). Furthermore, the GO fibers exhibit a remarkable 76% elongation and 17 J/m^3 tensile strength, allowing them to be twisted into a variety of structures (Fig. 4b IV). Moreover, Cao et al. produced graphene fibers using the thin film shrinkage method [69]. Special emphasis was placed on the features that the twisted fiber's distinctive spiral structure and high flexibility confer. For instance, the

spiral structure demonstrates a reversible resistance change during the stretching cycle. In addition, the abundant microchannel structure in the fiber endows it with a high liquid absorption capacity, resulting in a wide range of potential applications in the fields of sensors, energy producers, and artificial muscles.

Confined Hydrothermal Preparation of Graphene Fibers

As depicted in Fig. 4c I, the limited hydrothermal method is another essential way for preparing graphene fibers, similar to the hydrothermal method for preparing reduced GO aerogel. Under conditions of high-temperature, oxygen-containing functional groups on the surface of GO gradually degrade, and the electrostatic repulsion between GO lamellar gradually weakens, which is advantageous for assembling GO [70]. Qu et al. originally used this approach to manufacture graphene fibers in 2012, employing a capillary with an adjustable inner diameter [71]. After heating, rGO gel fibers were generated under capillary restrictions, and graphene fibers were created after additional drying and contraction. The resultant fibers are highly mechanically flexible and may be shaped into a variety of configurations. In addition, this hydrothermal approach demonstrates excellent operability. Correspondingly, multifunctional fibers can be easily fabricated by mixing functional nanomaterial with GO solution. Chen et al. produced CNT/rGO composite fibers with a nitrogen-doped hierarchical structure to reduce the π–π stacking effect of rGO sheets during hydrothermal reduction (Fig. 4c II and III) [64]. The uniform distribution of CNT within the fiber prevents the stacking of graphene sheets, allowing the composite fiber to exhibit a SSA of 396 m^2/g and a conductivity of 10,200 S/m. The large SSA and conductivity results in a large electrochemical active area (ion-accessible surface) and a capacitance of up to 305 F/cm^3. Owing to this outstanding electrochemical performance, the CNT/rGO composite fibers are able to power a variety of devices, such as ultraviolet (UV) photodetectors and light-emitting diodes.

Preparation of Graphene Fibers Using the Microfluidic-Spinning Method

Microfluidic-spinning differs from the wet-spinning and dry-spinning method as it involves the flow of multiphase fluids in microchannels with varying shapes. By constructing multiple channel forms and altering fluid composition and flow rate, quick prototyping, accurate structural control, and in situ chemical reaction are easily attainable in this method [72, 73].

Laminar flow in microchannels is essential for fiber preparation and is frequently affected by gravity, inertia, viscosity, and surface tension. Unlike the microfluidic-spinning technique that utilizes 1D macromolecules as precursors, the absence of intermolecular entanglement in GO solution leads to high viscoelasticity [65]. Meanwhile, as depicted in Fig. 4d I, the interfacial tension can be precisely regulated to produce microdroplets with varying aspect ratios by adjusting the surfactant concentration in the shell flow oil phase. Importantly, when the GO flow rate is extremely low, even though the interfacial tension between the GO phase and oil phase is very low, GO will spontaneously form microdroplets due to the long action time of the interfacial tension. In addition, by adding polyacrylate sodium (PAAS) to the GO solution to improve its tensile qualities, GO will transition from droplet to fibrous form. It is important to note that aqueous solutions can efficiently reduce the interfacial tension between GO solution and shell flow, which is advantageous for fiber creation. As depicted in Fig. 4d II, Qu et al. used an aqueous sodium alginate solution as the shell flow and a high-concentration GO solution (18 mg/mL) as the core flow to create GO fibers in microchannels [66]. The composite GO fibers were then put into an aqueous $CaCl_2$ solution to further coagulate them. With a rise in eccentric flow rate, the fibers exhibited an eccentric, sandwich, and reverse core structure in succession. This change in the morphology of the fibers is a result of the synergistic effect of the decrease in GO order resulting from the increase in GO flow rate and the cohesiveness of sodium alginate. Silva et al. simplified this process by using CTAB solution as shell flow and coagulation bath [74]. In addition, they discovered that the diameter of GO fiber could be modified by adjusting the velocity differential between the core and shell flow. As shell velocity increases gradually, the diameter of GO fibers drops exponentially. Moreover, as the compression effect on nuclear flow increases gradually, shell velocity increases. Due to the shortening of the diffusion length, the interaction period between CTAB and GO simultaneously decreases, which further promotes the formation of small-diameter GO fibers.

Preparation of Graphene Fibers by Chemical Vapor Deposition

Basically, the above-mentioned methods prepare graphene fibers via the top-down approaches with precures of graphite. On the contrary, CVD provides a bottom-up solution to prepare high quality graphene fibers [75]. Typically, in the graphene growth process of CVD method, precursor gas will decompose into carbon atoms or clusters at high-temperature environment [76]. Then these active reaction groups will reach adsorption desorption equilibrium on the surface of the substrate, and groups with higher adsorption energy will be retained. Finally, single layer or a few layers of graphene will be generated through the growth

mechanism of surface-mediated reactions or segregation [77]. It is worthy to point out that, the as-prepared single or few layers graphene normally present less defects compared with the modified Hummers method. In 2011, Li et.al extended this CVD method from graphene film to fiber [78]. First, the graphene film was spread on ethanol surface, under the action of surface tension, the edge of the film will gradually curl upward. Then, the graphene film is extracted from ethanol and shrinks into fiber with the evaporation of ethanol. The as-prepared graphene fiber presents a high electrical conductivity of 1000 S/m. Additionally, graphene fibers can be directly grown by changing the CVD growth substrate from two-dimensional films to one-dimensional fibers. Dai et al. selected copper wires as growth substrate for the CVD growing process [79]. The copper substrate was subsequently etched to generate hollow graphene fibers which present a high conductivity of 12,730 S/m. With precise controlling of molecular gas flow in confined space, Liu et al. further extended the growth substrate to quartz fiber [80]. The generated graphene-photonic crystal fiber presents a tunable light–matter interaction and broadband wavelength response. In this context, the flexible substrate selection in chemical composition and geometry endows CVD method a prospective preparation approach for defect-free and multifunctional graphene fibers [81].

Elemental Regulation of Graphene Fibers

The characteristics of graphene fiber/fabric electrodes largely depend on the properties of graphene sheets, which serve as the fundamental constituent of the fibers [82]. Bottom-up chemical and structural regulation methods can enhance the electrochemical/mechanical performance of graphene. The reported methods includes heteroatomic doping for electrochemical activity enhancement; pore size regulation for ion transport property enhancement; defect reparation for conductivity enhancement. Numerous studies on the relationship between element and fiber properties for high-performance flexible supercapacitors have been conducted thus far.

Heteroatom-Doped Graphene

Heteroatom doping is an effective method for regulating electron distribution in graphene sheets. Through altering the chemical valence of heteroatoms during charge and discharge, heteroatom doping can not only increase the conductivity of graphene sheets but also provide abundant electrochemical activity sites for graphene sheets [83]. For heteroatomic doping of graphene sheets, numerous techniques, including CVD [84], plasma [85], ball milling [86], thermal annealing [87], and solvent synthesis [88] have been

used to date. However, to ensure a smooth spinning process for graphene fibers, doping graphene sheets prior to or during spinning is desirable. Therefore, it is challenging to apply techniques such as ball milling and CVD to the elemental doping of graphene fibers.

As a result of the restricted space and the hydrothermal process, the confined hydrothermal approach has many benefits for producing graphene fibers doped with heteroatoms. Wu et al. synthesized nitrogen-doped graphene fibers using a two-step confined hydrothermal method, as shown in Fig. 5a I [89]. First, urea was used as a nitrogen source, followed by the hydrothermal preparation of amino-modified GO fibers. The amino group was subsequently broken down by thermal annealing at high temperatures, with nitrogen atoms entering the graphene framework. Small levels of nitrogen doping are believed to greatly improve the conductivity, porosity, and activity of fibers. The pseudocapacitance provided by a nitrogen atom is derived from the Faraday reaction between the unpaired electrons of pyrrole N and pyridine N and the hydrogen ions in the electrolyte (Fig. 5a II). However, excessive nitrogen doping will destroy the sp2 carbon skeleton of graphene which leads to a lower electrical conductivity, resulting in a decrease in specific capacitance. In this context, it is necessary to precisely control the content of heteroatoms to exploit synergetic effect between active heteroatoms site, electrical conductivity, and porous network for high-performance flexible fiber electrode.

Frustratingly, after heteroatomic doping, the spinning performance of doped GO often decreases drastically, limiting bottom-up heteroatomic doping and continuous synthesis of graphene fibers. As shown in Fig. 5b, Wang et al. discovered that GO itself may be employed as a binder for spinning, thereby enhancing the spinning performance of the spinning solution [90]. In their research, allyl thiourea and GO were hydrothermally treated principally to create N, S-doped 3D rGO aerogel, which cannot be successfully spun due to the significant contact force between N, S-doped rGO sheets. The addition of 5% untreated GO can significantly improve the ability of N, S-doped rGO to spin continuously. N and S atoms penetrate the graphene skeleton after further heat annealing, improving the electrical conductivity and electrochemical activity of the fibers.

Regulation of GO Pore Structure

Monolayer graphene has a SSA of 2630 m^2/g and high quantum capacitance; however, the strong π–π stacking effect between graphene easily causes the restacking structure of graphene fiber, leading to a decrease in electrochemical active area and hysteresis in ion migration. The pores in the graphene sheet can improve the SSA of graphene fibers and decrease the ion transport distance. As depicted in Fig. 5c, Zhu et al. etched 1–10 nm-sized nanopores on the
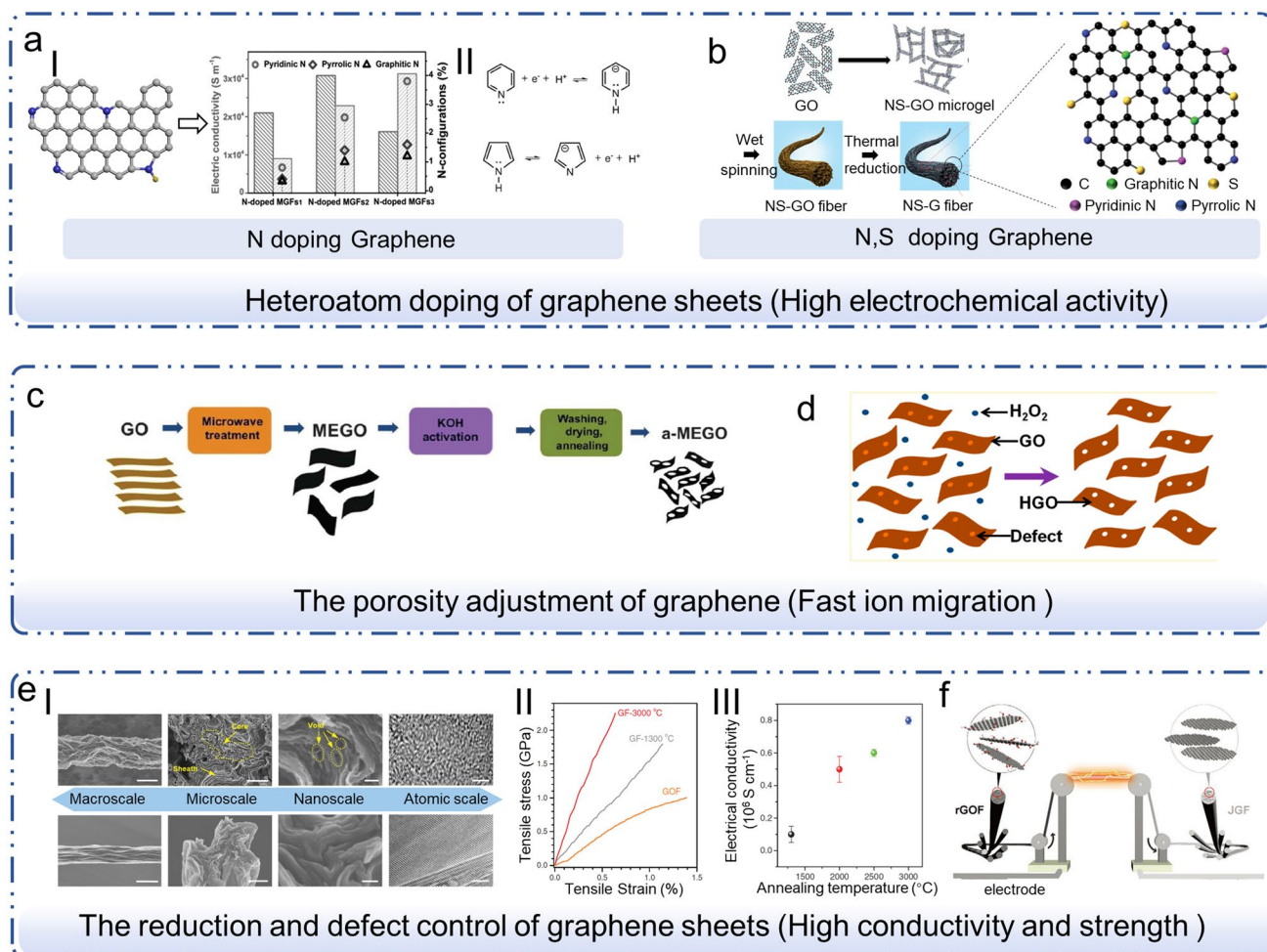
Fig. 5 Elemental regulation of graphene fibers/fabrics. **a** N doping graphene: I. the relation between different nitrogen-active sites and electric conductivities; reproduced with permission from Ref. [89], Copyright 2017, Wiley; II. Faraday reaction between unpaired electrons N and hydrogen ions; reproduced with permission from Ref. [91], Copyright 2021, Wiley. **b** N, S-doping graphene; reproduced with permission from Ref. [92], Copyright 2015, Royal Society of Chemistry (RSC). **c** Chemical activation of GO with KOH; reproduced with permission from Ref. [93], Copyright 2011, AAAS **d** Schematic illustration of formation mechanism of porous GO; reproduced with permission from Ref. [92] Copyright 2015, ACS. **e** High-temperature annealing of graphene fiber: I. Multiscale structures of graphene fiber; II. Typical tensile stress curves of graphene fibers; III. The electrical conductivity of GFs annealed at different temperatures; reproduced with permission from Ref. [94], Copyright 2016, Wiley. **f** Graphene fibers fabricated using the dynamic Joule heating method; reproduced with permission from Ref. [95], Copyright 2022, Wiley

surface of graphene in 2011 using KOH as an etching agent at high temperatures [93]. N_2 adsorption/desorption measurements indicate that graphene has a SSA of up to 3100 m^2/g. These 3D pores significantly improve the electrochemical characteristics of graphene, resulting in a capacitance of 200 F/g and good rate performance that demonstrates the effectiveness of the chemical etching process. However, due to the high temperature of the etching process, graphene sheets etched with KOH can no longer scatter in water, rendering them unsuitable for spinning. Hence, the key to prepare porous GO is to identify an adequate etching agent that maintains the water solubility of GO after etching [96]. Kamat et al. discovered that Au can catalyze H_2O_2 to generate OH· and etch GO when exposed to UV irradiation [97]. Subsequently, Duan et al. demonstrated that H_2O_2 can successfully etch and reduce GO to produce rGO aerogel with a 3D porous structure at high temperature and high pressure, even in the absence of Au and UV [98]. This procedure was further simplified by Duan et al. Correspondingly, it was found that H_2O_2 can successfully etch GO in a 95 °C water bath (Fig. 5d). The as-prepared GO retained good water solubility, allowing for the effective fabrication of graphene films [92]. Recently, Qiu et al. combined this process with the restricted hydrothermal method to produce graphene fibers with a porous structure that exhibits exceptional electrochemical characteristics [99]. However,

concerns such as uncontrollable pore size and high reduction degree of GO still need to be resolved, necessitating the discovery of a suitable etching agent and etching process.

Reparation of Graphene Defects

Electrical conductivity and mechanical strength are two motivating elements for increasing the electrode characteristics of graphene fiber/fabric. According to Griffth's criterion, the mechanical strength of brittle materials is governed by the size and placement of randomly distributed defects. After chemical and thermal reduction at low temperature, the surface of rGO still contains flaws, and oxygen-containing functional groups, resulting in a loss in the mechanical characteristics and electrical conductivity of the fiber electrode. To solve this problem, Gao et al. developed corresponding defect remediation approaches [94]. As depicted in Fig. 5e I, large lateral size GO was used as spinning precursor to reduce the edge defects of fiber. Then, a multistage stretching method was used to increase fiber orientation. Finally, a high-temperature thermal annealing method was adopted to rearrange the carbon atoms on graphene sheets to reduce the defects in graphene sheets. The optimized graphene fibers possess a tensile strength of 1.45 GPa and conductivity of 0.8×10^6 S/m (Fig. 5e II and III). In addition, Liu et al. devised a method of continuous regulation based on the Joule heat effect for eliminating graphene fiber defects [95]. As depicted in Fig. 5f, the Joule heating impact of current repairs graphene lamellar flaws in a short amount of time (20 min at ≈2000 °C) with a modest amount of energy (≈2000 kJ m^{-1}). Compared to traditional thermal annealing, Joule annealing produced a material with a higher Hermann orientation factor (0.73), conductivity (5.9×10^5 S/m), and tensile strength (1.07 GPa).

Cross-section Morphology and Nano-/Micro-structure Regulation of Graphene Fibers

Cross-sectional Morphology Regulation of Graphene Fibers

Taking advantages of different spinning methods, graphene fibers with distinct cross-sectional morphologies can be produced for a variety of applications. Fiber cross-sectional morphology can be roughly categorized as hollow structure, ribbon structure and twisted structure. The excellent electrochemical performance of the device is a result of the porous structure and the ion adsorption/desorption capability of the fiber. The ribbon shape offers benefits in terms of the OD of graphene sheets and mechanical properties of the fibers. On the other hand, the exceptional tensile strength and pliability

of twisted fibers agree well with the ultra-flexible application scenarios.

Hollow Graphene Fibers

Based on the energy storage method of EDLC, a large SSA can provide more ion adsorption sites to boost electrode specific capacitance. For this purpose, Peng et al. demonstrated that if a fiber has a hollow structure, the hollow structure within the fiber can provide increased SSA, enhance the electrode/electrolyte contact, and facilitate charge transfer [100]. As depicted in Fig. 6a, graphene fibers with hollow structures were synthesized using a restricted hydrothermal approach based on the gas-generating properties of GO during heating. Simultaneously, poly(3,4-ethylened ioxythiophene):polystyrenesulfonate (PEDOT:PSS) was added to the GO solution, and its hydrophilic group enhanced the diffusion of GO, resulting in the production of hollow graphene fibers. This unique hollow shape is advantageous for enhancing the electrode/electrolyte contact interface, resulting in a capacitance of 143.3 F/cm^3 and satisfactory mechanical properties.

In comparison to the confined hydrothermal method, the wet-spinning method is simpler to implement on a large scale. However, due to the shearing force of the spinneret, GO sheets tend to disperse along the axial direction during the wet-spinning process. Meanwhile, the restacked structure predominated due to the strong van der Waals force between the GO sheets, which is not conducive to the smooth movement of ions. This phenomenon could be prevented by selecting an appropriate coagulation bath. As depicted in Fig. 6b, an increase in the solidification rate of GO in the coagulation solution would alter the dense structure of the fiber into a porous one [61]. In particular, a dense structure was observed when a CaCl$_2$ aqueous solution with a slower coagulating velocity was utilized as the coagulation bath. In the event of a moderately coagulating acetic acid coagulation bath, big holes developed in the fiber. Interestingly, when acetone is used as the coagulation bath, the porous network fiber is finally formed because of the low viscosity, high fluidity, and rapid diffusion rate of acetone. The water in gel-state fibers can be rapidly released, and the residual acetone evaporates in a short period of time, which inhibits the restacking of graphene. Furthermore, during the reduction process, the high-temperature thermal reduction can also suppress the restacked structure of GO sheets. Correspondingly, the final SSA of the fiber electrode was estimated to be 2210 m^2/g, with a specific capacitance of 409 F/g.

Ribbon Structure Graphene Fibers

Compared to graphene fibers with a circular cross section, the ribbon structure has a shape that is more compatible,
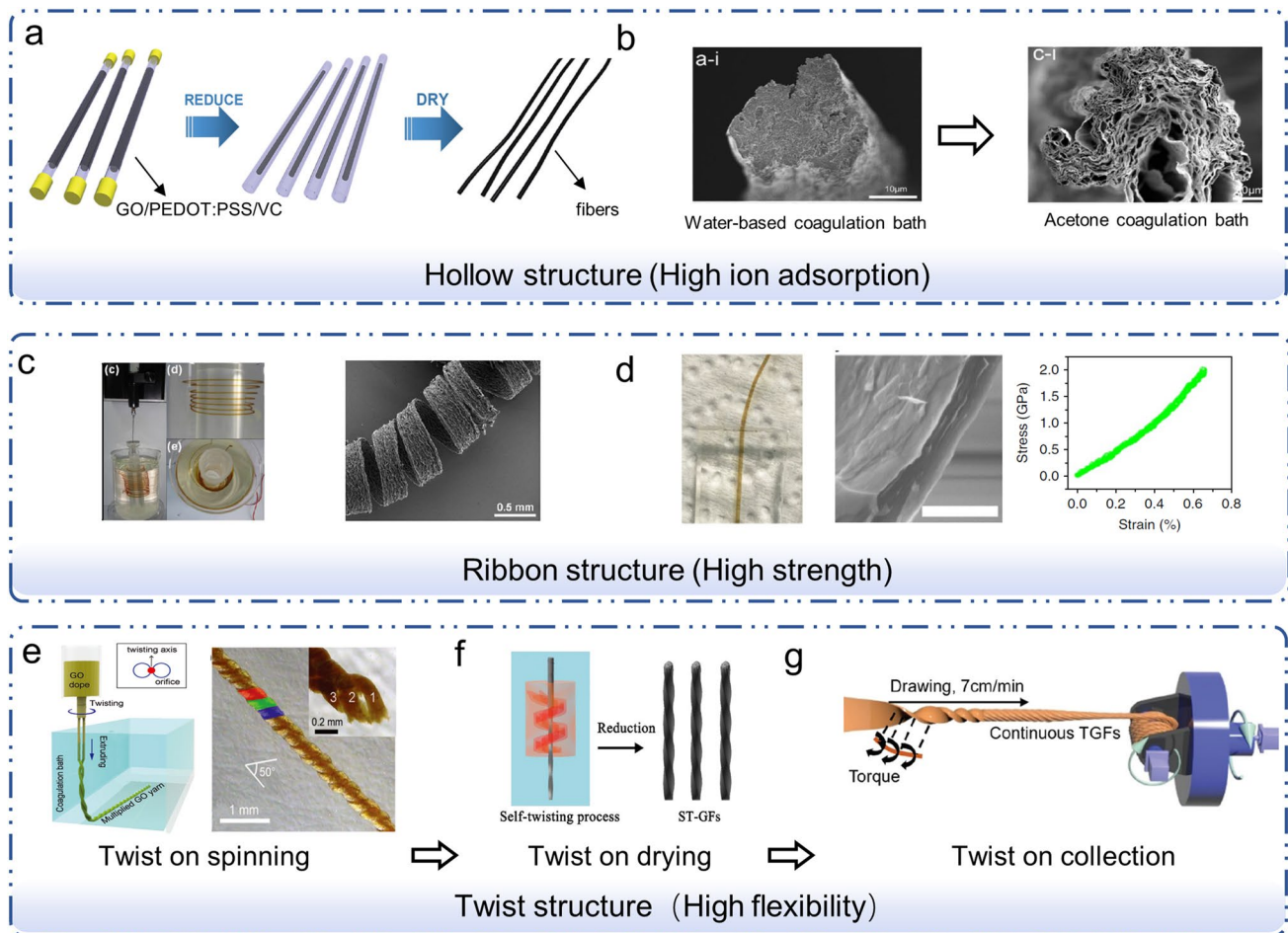
Fig. 6 Cross-sectional morphology regulation of graphene fibers. **a** Preparation of hollow-structured graphene fibers and its formation mechanism; reproduced with permission from Ref. [100], Copyright 2016, Wiley. **b** Evolution of fiber structure in different coagulation baths; reproduced with permission from Ref. [61], Copyright 2014, ACS. **c** Illustration of preparation process of ribbon structure fiber and its SEM images; reproduced with permission from Ref. [101], Copyright 2013, ACS. **d** Wet-spinning of ribbon structure fiber with high mechanical strength; reproduced with permission from Ref. [73], Copyright 2019, NPG. **e** In situ wet-spinning of twist structure graphene fibers; reproduced with permission from Ref. [102], Copyright 2017, RSC. **f** Dry-spinning of twisted structure graphene fibers; reproduced with permission from Ref. [103], Copyright 2019, Elsevier. **g** Continuous drawing–twisting fabrication process of twisted graphene fibers; reproduced with permission from Ref. [104], Copyright 2019, RSC

which is advantageous for improving OD and decreasing interlayer defects. Therefore, the ribbon structure fiber tends to exhibit greater mechanical capabilities and superior twisted durability, both of which are essential for practical wearable devices [73].

Cao et al. generated ribbon graphene fiber, as depicted in Fig. 6c, by applying shear stress on GO fiber in a rotating chitosan aqueous solution coagulation bath. The resulting ribbon fibers exhibit a width-to-thickness ratio of 100 as well as exceptional mechanical strength and flexibility. Impressively, after 275% stretching, it was able to fully recover, demonstrating its commendable mechanical weaving properties. Accordingly, it can be easily woven into fabrics with various topologies, making it a potent application substrate for flexible sensing and fiber energy storage [101].

Rotating coagulation bath is a viable approach for producing graphene fibers with a ribbon shape; however, the OD of graphene sheets is still low. As illustrated in Fig. 6d, Lian et al. designed a spinneret that is compatible with GO and has flat internal channels [73]. By manipulating the aspect ratio of the spinneret channel, it is possible to alter the orientation of the GO fiber. Consequently, the improved fiber demonstrated a remarkable strength of 1.9 GPa. These graphene fibers with an anisotropic ribbon structure offer a novel way to control the OD of graphene, thereby increasing the strength of the fibers.

Twisted Graphene Fibers

Graphene fibers with a twisted structure have an exceptional tensile elasticity, as demonstrated by Terrones et al. using the thin film contraction method [63]. However, the two-step process of scraping and twisting required to produce twisted graphene fibers is complex and not favorable for continuous fiber production. Therefore, spinning is required for realizing continuous fabrication process. Correspondingly, the fibers can be twisted in three simple steps: (1) twisting at spinneret: twisting the gel fibers after the spinning solution is ejected out of the spinneret; (2) twisting during drying process: twisting gel fiber during drying process; and (3) twisting during the collection process: twisting the fiber during the fiber collection process.

In the spinning process, a rotating spinneret is the most straightforward approach to produce twisted graphene fibers. As shown in Fig. 6e, Li et al. fabricated twisted graphene fibers by controlling the rotation rate of the spinning nozzle and the collection rate of the solidification bath. The breaking elongation of twisted fiber at 257 twists/m was 7.3%, tensile strength was 186 MPa, and toughness was 6.1 MJ/m [102]. Additionally, the dry-spinning method is used to provide twist to the drying process. As shown in Fig. 6f, Chen et al. injected the GO gel fibers into a high-temperature drying chamber and then twisted the fibers through a cyclone drying air flow, that was parallel to the spinning direction [103]. The twisted fiber has a high elongation at break of 26.3% and high tensile strength of 244.8 MPa, which is beneficial to the mechanical flexibility of the assembled fiber supercapacitor. During the spinning and coagulation processes, the fibers are not completely coagulate, leading to the in situ twist. However, these twisted threads are typically tightly bonded and difficult to unravel. This issue can be avoided by twisting during the collection phase. Accordingly, graphene fibers can be twisted during collection by combining the wet-spinning method with the twisting procedure [104]. As illustrated in Fig. 6g, Fang et al. first developed shear-resistant ribbon GO fibers. Then, a twisting-drawing device is connected to the end of the continuous production device, allowing the fibers to be simultaneously twisted and collected. The as-prepared chiral twisted graphite fiber possesses a high breaking elongation of 29% and tensile strength of 130 MPa and has potential applications in artificial muscle fields.

Nano-/Micro-structure Regulation of Graphene Fibers

Improving the energy density of the fiber requires a hierarchical pore structure, high electrical conductivity, and high electrochemical activity. Due to the strong π–π stacking effect of graphene sheets, pure graphene fibers often exhibit a densely stacked structure, despite the enormous SSA of single-layer graphene sheets. This decreases not just the quantum capacitance of the graphene sheet but also the ion adsorption and transport capacity of the electrode. Meanwhile, the limited number of electrochemically active sites on the graphene surface diminishes the charge storage capacity of the electrode. Taking advantage of different assembly methods may successfully transform the ordered structure of graphene fibers into a porous structure, which inhibits the restacked structure, increases the SSA, and generates the transport channel for electrolyte ions. In contrast, the exceptional compatibility of graphene fibers makes it simple to combine them with active substances, which is crucial for enhancing the energy density of fiber supercapacitors.

Ordered Structure

As a typical non-Newtonian fluid, GO solution is simple to organize along the shear stress direction. Based on this, Gao et al. proposed a continuous stretching method in which GO gel fibers were stretched in segments and the OD was improved gradually under tensile shear force (Fig. 7a) [94]. The results of small-angle X-ray scattering demonstrated that graphene fibers had an OD of 81% and ultra-high strength of 1.45 GPa. Alternatively, it appears that the structure of spinning microchannels will similarly affect the OD of graphene fibers. The tension flow generated by the conical channel can greatly enhance the mechanical strength of fibers by increasing the OD [73]. Remarkably, as seen in Fig. 7b, GO was able to attain vertical orientation under the expansion flow induced by the abrupt expansion channel, allowing the fabrication of graphene fibers with a vertical orientation. Previous study has demonstrated that such a vertical orientation structure can significantly shorten the ion transport path in an electrode and improve its electrochemical performance [109]. The aforementioned investigations present that managing the fluid flow is an effective strategy that can not only regulate fiber OD but also the direction of sheet arrangement to effect the transformation of fiber orientation from axial to vertical. This offers a novel method for constructing effective ion channels and achieving efficient ion transport and adsorption.

Hierarchical Porous Structure

Pure graphene fiber has a SSA of only 13 m^2/g due to the layered structure of graphene sheets [110]. Therefore, the precise design of fiber pore structure comprises a critical strategy to improve the charge storage and ionic transport of fiber electrode. Based on the location of pores, porous structures can be roughly classified as surface porous structures or internal porous structures. For surface porous architectures, the core of graphene fibers is often left intact to
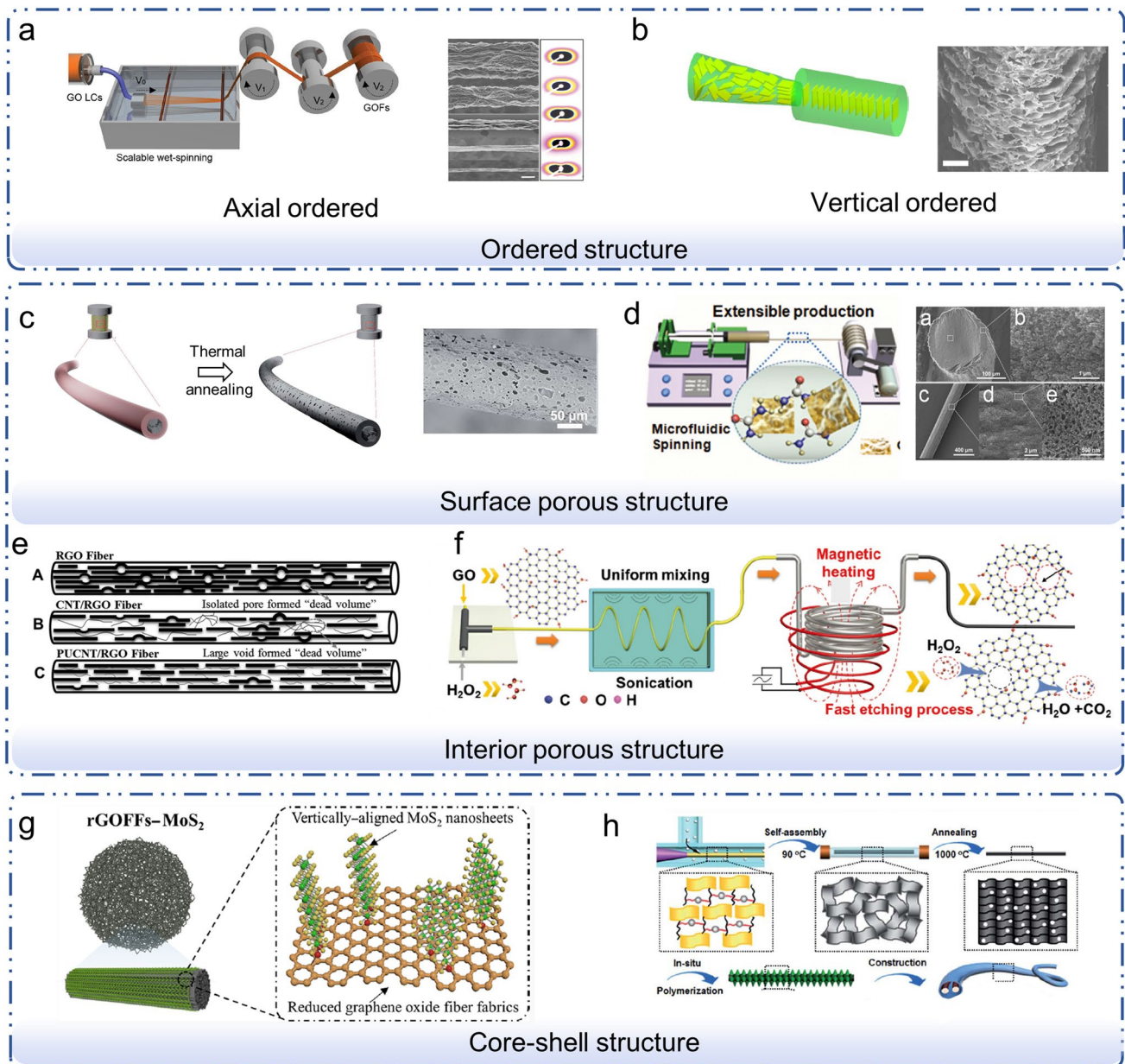
Fig. 7 Nano-/micro-structure regulation of graphene fibers. **a** Continuous stretching of GO fibers; reproduced with permission from Ref. [94], Copyright 2016, Wiley. **b** Vertically aligned graphene fibers; reproduced with permission from Ref. [73], Copyright 2019, NPG. **c** The thermal annealing process and SEM image of porous fibers; reproduced with permission from Ref. [105], Copyright 2018, RSC. **d** The microfluidic-spinning process of porous nitrogen–doped graphene fiber; reproduced with permission from Ref. [89], Copyright 2017, Wiley. **e** Illustration of the dead volume of graphene fibers; reproduced with permission from Ref. [106], Copyright 2021, Wiley. **f** Illustration of the magneto–thermal microfluidic-assisted synthesis of multiscale microfibers; reproduced with permission from Ref. [99], Copyright 2020, Wiley. **g** Illustration of the MoS_2/graphene core–shell fiber–based fabric; reproduced with permission from Ref. [107], Copyright 2022, ACS. **h** The synthesis process of polyaniline nanorod arrays/graphene composite fibers; reproduced with permission from Ref. [108], Copyright 2018, RSC

provide basic mechanical qualities and electrical conductivity, whereas the exterior is porous to increase the SSA of the electrode. As illustrated in Fig. 7c, Wang et al. covered the surface of GO fibers with a mixture of GO and phenolic glue, which degraded into porous structures when subjected to high temperatures. This porous graphene fiber

with a core–shell structure has a SSA as high as 416.4 m^2/g (88–97% micropores, 0–8.3% mesopores, and 1.9–4.2% Macropore) [105]. Chen et al. integrated element doping with pore structure modulation, as seen in Fig. 7d. Urea was used as a N source to prepare N-modified GO fiber using the microfluidic-spinning method, followed by high-temperature

annealing method to create a porous fiber surface. The as-prepared fiber has a SSA of 388.6 m^2/g and pore size range ranging from 2.4 to 190.5 nm. Due to its porous structure, a high specific capacitance of 1132 mF/cm^2 and energy density of 95.7 μWh/cm^2 were attained [89].

To maximize the porosity usage of the fiber electrode, it is preferable to have an internal porous structure. Effective method for manufacturing internal porous graphene fibers is to introduce a spacer into the fiber to increase the layer spacing between graphene sheets, thereby creating more ion channels. Based on the wet-spinning method, the preparation process is straightforward and it is simple to establish mass production. In addition, the restacking effect of graphene sheets can be considerably prevented by employing appropriate barrier materials. As illustrated in Fig. 7e, Zhu et al. discovered that unzipped carbon nanotubes inhibited the stacking of graphene sheets and decreased the viscosity of GO solution. Consequently, it appears that the dead volume generated by phase separation during coagulation is less [106]. In addition to having outstanding mechanical properties (a tensile strength of 134.4 MPa), the produced fibers also have a high SSA (268.2 m^2/g). Similar barriers consist of activated carbon [110], CaCO$_3$ [111] and others. In addition, the ion transport capacity and electrochemical activity of the fiber can be increased simultaneously by choosing a barrier with a higher electrochemical activity, such as MXene [7], and MoS$_2$ [112].

Designing and fabricating 3D porous network graphene fibers with a hierarchical structure is yet another excellent method for achieving an interior porous structure. The 3D network has a shorter ion migration channel than the previous method, which provides graphene fibers greater ion storage and transit capacity. As shown in Fig. 7f, Wu et al. used magneto–thermal microfluidic technology to oxidize and etch GO with H$_2$O$_2$ to produce graphene fibers with an interior porous network structure [99]. Core–shell graphene fibers with a 3D porous structure were produced by carbonizing ZIF-8 on the surface of the fibers. The CP/HG fiber contains an open internal porosity ion channel, large SSA (569.4 m^2/g), and moderate concentration of nitrogen-active sites, which facilitate the migration and accumulation of ions. The improved fibers have an exceptional specific capacitance of 2760 mF/cm^2 and remarkable breaking strength of 300 MPa.

Core–Shell Structure

Core–shell structure fiber consists of two components: the intercore layer and the shell layer that encases the core. The core layer is typically composed of graphene fiber, whereas the shell layer is composed of a range of components with distinct properties. The shell layer can be roughly classified into the following categories: (1) porous shells, include

graphene aerogel [113] and porous graphene [114]; (2) pseudocapacitance shells, such as MoS$_2$, [115] MnO$_2$, [116] and conductive polymers [117]; (3) Functional shells, such as sodium carboxymethyl cellulose(CMC) [118]. The porous shell increases the SSA of the composite fiber and enhances ion adsorption and transport. Correspondingly, the pseudocapacitive material significantly enhanced the electrochemical activity of the composite fibers including graphene fibers in the core layer while maintaining their high electrical conductivity. Functional shells confer extensive functionality to the fiber. Using coaxial spinning technology, Gao et al. coated electrical insulating CMC layers on graphene fibers, which effectively suppressed the short circuit phenomenon of graphene fiber supercapacitors [118].

To date, a variety of methods including hydrothermal [116], electrochemical deposition [113], microfluidic spinning [72], and coaxial spinning [118] have been developed to fabricate core–shell structure fibers. As shown in Fig. 7g, Guan et al. [107] introduced MoS$_2$ nanosheets to the surface of a graphene fiber–based fabric using improved hydrothermal-assisted assembly techniques. After reduction, the MoS$_2$ nanosheets are in situ attached to the graphene carbon skeleton by C–O–Mo covalent connections, yielding the core–shell structure MoS$_2$/rGO fiber. The in situ vertical covalent bridge and appropriate pseudocapacitive reactivity of MoS$_2$ result in the excellent mechanical stability and outstanding electrochemical performance of the composited fiber–based fabric. Similarly, Kim et al. additionally loaded a layer of WO$_3$ on the surface of graphene fiber using the hydrothermal method and then prepared WN-rGO composite fiber by nitriding. The addition of WN significantly increased the specific capacitance of the composite fiber, which was 7.5 times that of graphene fiber alone [119]. Simultaneously, as depicted in Fig. 7h, Wu et al. generated graphene fibers by microfluidic-spinning method and then in situ manufactured polyaniline nanorod arrays utilizing their surface-based electrochemical deposition technique. The conductivity and specific capacitance of the obtained composite fibers reached 18,734 S/m and 230 mF cm^{-2}, respectively [108]. According to Meng et al., combining the porous structure and core–shell structure can further improve the electrochemical performance of an electrode. Based on the microfluidic-spinning method, Meng et al. used monogenerated 3 polyamidoamine dendrimer–coated polystyrene as a template to fabricate internal porous graphene fibers. Subsequently, vertical NiO nanosheets were grown on the surface of porous graphene fibers by microchannel-assisted hydrothermal synthesis. The core–shell composite fiber had a hierarchical porous structure with a SSA of 425.6 m^2/g and conductivity of 17,660 S/m. Meanwhile, the NiO nanosheet with a vertical shell demonstrated high electrochemical activity, which endowed the composite fiber with a capacitance of 605 mF/cm^2. In this regard, core–shell

structure is proved to be a crucial architecture for enhancing the electrochemical performance of fiber supercapacitors [120].

In general, electrochemical and applicable mechanical performances are two predominant criterions for high-performance graphene-based fiber supercapacitor. Accordingly, their respective influencing factors and implementation approaches are summarized in Table 1 for the guidance to further research. Briefly, high SSA, high electrochemical activity and conductivity are prerequisite for high energy/power density. In this context, it is essential to select corresponding fabrication method, including wet spinning, dry spinning, thin film shrinkage, confined hydrothermal, chemical vapor deposition, microfluidic spinning, to regulate fiber morphology and structure. Additionally, from the perspective of applicable mechanical features, dry spinning, wet spinning, thin film shrinkage and chemical vapor deposition are suitable to prepare twisted, ribbon and order structure fiber with high flexibility/strength.
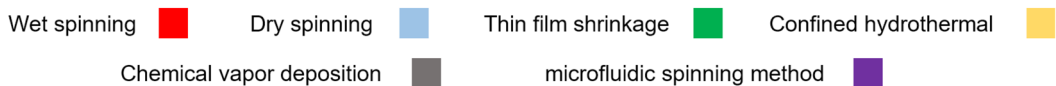
Preparation of Graphene Fiber Fabric

Due to their high electrical conductivity and chemical stability, carbon fiber fabrics such as carbonized biomass carbon cloth [121] and carbon fiber fabrics [122] have been widely utilized as electrode materials for flexible supercapacitors. Hu et al., for instance, produced $NbOPO_4$ nanosheets on carbon fabric in oxalic acid solution and measured energy and power densities of 122.2 and 589.7 W/kg, respectively. However, further application is hampered by the comparatively modest SSA and electrochemical activity [122]. As depicted in Fig. 8a, graphene fiber fabrics are woven from graphene fibers. Thus, it inherits the fundamental characteristics of graphene fibers, including high electrical conductivity, high SSA, and high compatibility. Graphene fiber fabrics have greater electrical conductivity, active substance compatibility, ion diffusion capacity, and conduction compared to metal films, carbon fiber fabrics, and carbon nanofiber films. Consequently, it has become a highly competitive substrate candidate for the fabrication of fabric supercapacitors [123].

Mechanical weaving of graphene fiber is an effective and direct approach to prepare graphene fiber fabric. However, single graphene fiber normally presents limited spinnability. To this end, Razal et al. created GO fiber fabric by combining GO fiber with nylon fiber [19]. However, the produced GO fabric exhibited a loose structure and is therefore unsuitable for use as a flexible electrode. In this case, as depicted in Fig. 8b, high-toughness graphene fiber with ribbon topologies is excellent for constructing compact structure fabrics with a range of shapes [101].

Table 1 The summary and correlations of supercapacitor performance, fiber properties, Morphology and structure regulation and preparation methods

	Capacitor Properties	Fiber Properties	Morphology and structure regulation	Preparation methods
High performance graphene based fiber supercapacitor	High energy/ power density	High SSA	Hollow structure	🟨
			Hierarchical porous structure	🟥 🟪 🟨
		High electrochemical activity	Heteroatom doping	🟥 🟪 🟨
			Core-shell structure	🟦 🟥 🟩
		High conductivity	Heteroatom doping	🟥 🟨 🟪
			Defects regulation	🟥 🟦 🟩 🟨 ⬛ 🟪
	Applicable mechanical features	High flexibility	Twisted structure	🟦 🟥 🟩
		High strength	Ribbon structure	🟥 🟪
			Order structure	🟥 ⬛ 🟪

Wet spinning 🟥   Dry spinning 🟦   Thin film shrinkage 🟩   Confined hydrothermal 🟨

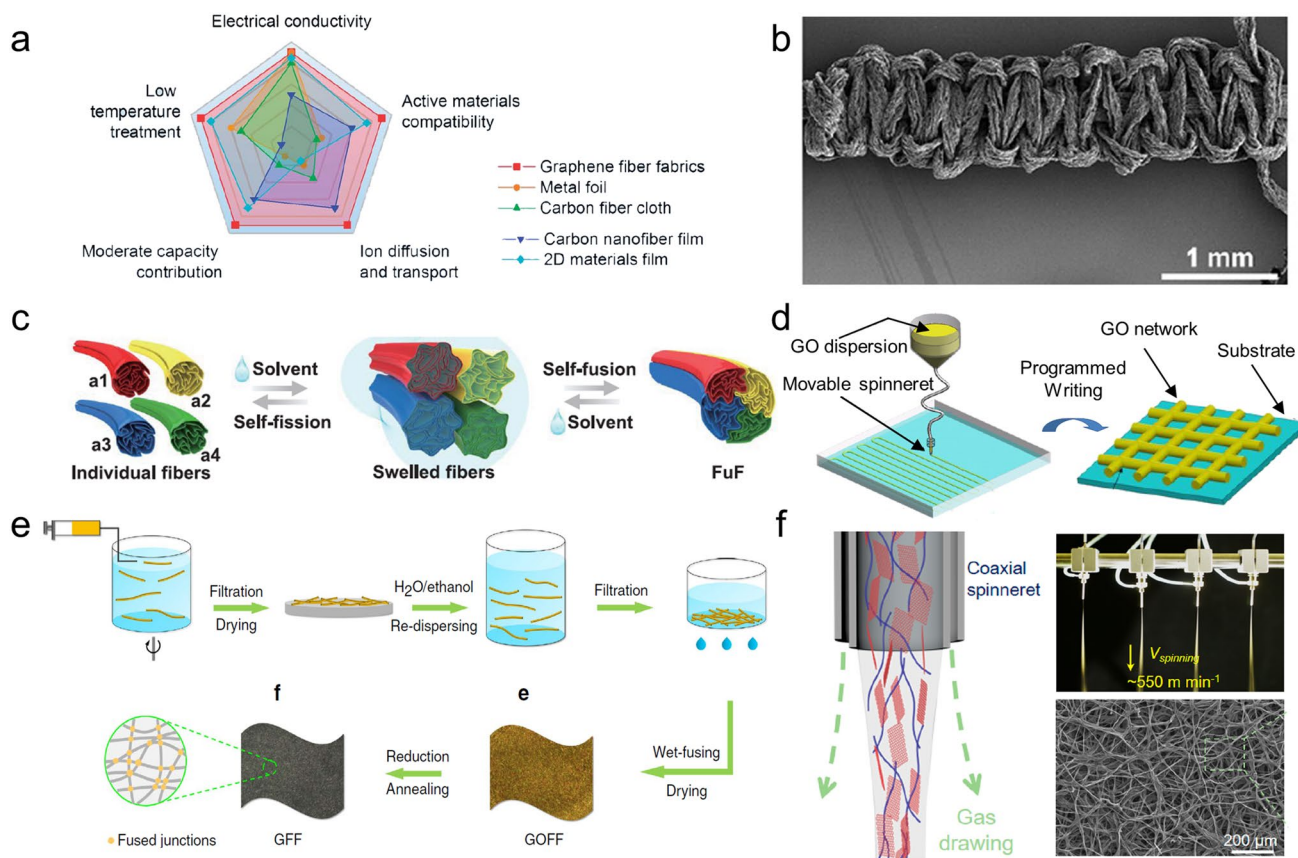Chemical vapor deposition ⬛   microfluidic spinning method 🟪

Fig. 8 Preparation of graphene fiber fabric. **a** Comprehensive performance comparison of various flexible substrates; reproduced with permission from Ref. [123], Copyright 2020, RSC. **b** Graphene fiber fabric woven by ribbon graphene fibers; reproduced with permission from Ref. [101], Copyright 2013, ACS. **c** Schematic illustration of the solvent triggered reversible self-fusion and self-fission of GO fibers; reproduced with permission from Ref. [124], Copyright 2021, AAAS.

d Programmable writing of fibers; reproduced with permission from Ref. [59], Copyright 2014, ACS. **e** Fabrication of graphene fiber fabrics via wet-fusing assembly; reproduced with permission from Ref. [125], Copyright 2016, NGP. **f** Schematic illustration of the blow spinning of graphene fiber fabrics; reproduced with permission from Ref. [126], Copyright 2021, ACS

The self-fusion behavior of GO fibers in polar solvents provides another solution to prepare graphene fiber fabric. As depicted in Fig. 8c, the fusion behavior is governed by the dynamic geometric deformation of the GO fiber shell, which is generated through solvent evaporation and infiltration. This reversible fusion-splitting method can be used to adaptably modify the dynamic structure of the fibers, generate fusible fibers with variable diameters, and regulate the merging and releasing of various guest materials [124]. Basing on this self-fusing behavior, dense graphene fiber fabric with porous network can be prepared followed by mechanical, thermal, or chemical reinforcement. As shown in Fig. 8d, Li et al. developed a direct writing technique to fabricate GO fibers fabrics where a programmable spinneret is adopted to control the movement of the GO solution to form a gel network of GO fibers [59].

Going beyond this certain, as shown in Fig. 8e, Gao et al. prepared graphene fiber non-woven fabrics with the reinforcement filtrating [125]. The wet-spinning method

was used to produce GO gel staple fibers, which were then filtered to form the gel network of GO fibers. Specifically, the degree of fiber fusion can be manipulated by adjusting the surface tension between fibers. After drying and thermal annealing, the textiles exhibit superior pliability and conductivity (2.8×10^4 S/m). This fabric has a high application potential for oil–water separation, electric heating film, and flexible energy storage due to its net-like structure and excellent mechanical qualities. Moreover, blast spinning can improve the preparation efficiency of graphene fibers for nonwoven materials. As depicted in Fig. 8f, Liu et al. added poly (acrylic acid) sodium with a high molecular weight to GO solution to improve the tensile properties of GO solution and enable the continuation of the high-speed blow-spinning process. Benefiting from the aid of high-velocity gas in the spinning process, the production speed of blow-spinning may reach 556 m/min, which is two orders of magnitude quicker than wet-spinning. This high efficient preparation method promises the

large-scale manufacturing of nonwoven graphene fibers fabrics [126].

Application of Flexible Supercapacitors

Flexible Energy Storage Applications of Fiber Supercapacitors

The fiber-shaped flexible supercapacitor can be built in three distinct configurations: (1) Fig. 9a, twisted structure supercapacitor; (2) Fig. 9b, parallel structure supercapacitor: the positive and negative electrodes are arranged in parallel or are twisted together; and (3) Fig. 9c, coaxial structure supercapacitor: positive and negative electrodes are wrapped around the same fiber [127]. Consequently, because of the simple structure and convenient preparation process, parallel or twisted supercapacitors are most commonly utilized due to their simple construction and simple preparation technique. In addition to energy density, mechanical quality is a crucial criterion for evaluating the performance of flexible supercapacitors. For this purpose, Zhi et al. proposed three parameters to quantitative analysis the flexibility of the device, including bending angle (θ), bending radius (R), and device length (L) [128]. When the bending angle and bending radius are determined, the stress area is inversely
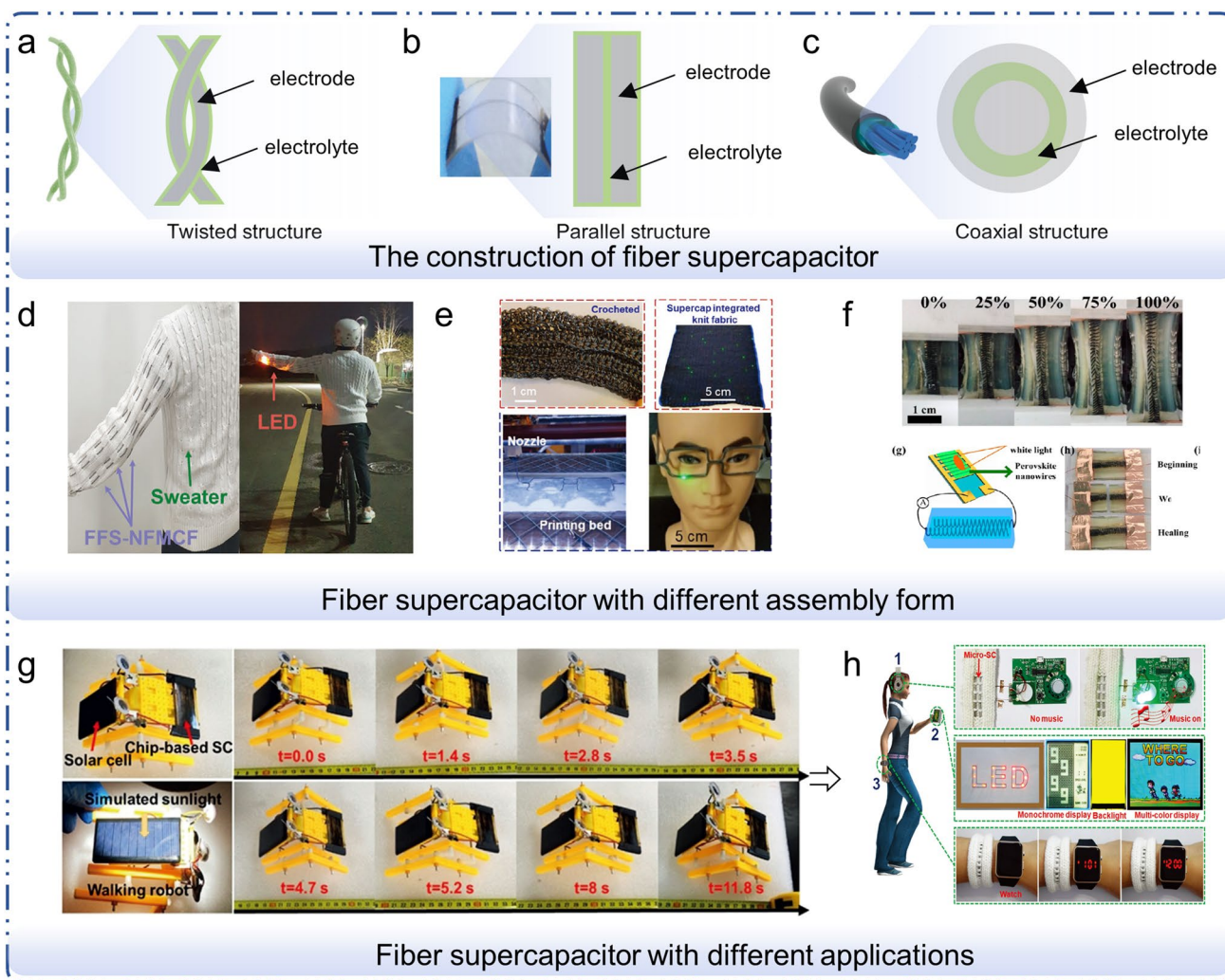

Fig. 9 Application of fiber supercapacitors in flexible energy storage. Schematic illustration of **a** twisted, **b** parallel, and **c** coaxial structure fiber supercapacitor; reproduced with permission from Ref. [64], Copyright 2014, NPG; reproduced with permission from Ref. [127], Copyright 2013, ACS. **d** Fiber supercapacitor that can be woven in sweater to power LED; reproduced with permission from Ref. [129], Copyright 2021, Wiley. **e** Machine weaving and 3D printing of fiber supercapacitor; reproduced with permission from Ref. [130], Copyright 2020, Wiley. **f** Photographs of self-healing fiber supercapacitor; reproduced with permission from Ref. [131], Copyright 2017, ACS. **g** Photographs of a self-powered walking robot powered by fiber supercapacitor; reproduced with permission from Ref. [99], Copyright 2020, Wiley. **h** Schematic illustration of wearable electronics powered by fiber supercapacitor; reproduced with permission from Ref. [89], Copyright 2017, Wiley

proportional to the length of the device. Additionally, when the bending radius and bending length of the device are specified, the stress area increases linearly with the bending angle. Therefore, a fiber with a greater aspect ratio can lower the stress concentration to the greatest extent possible. From this perspective, the 1D structure of the fiber supercapacitor facilitates its combination with fabric. As depicted in Fig. 9d, An et al. synthesized F, N co-doped carbon fiber and weaved it into everyday apparel to power LEDs, demonstrating the superior wearability of fiber supercapacitors [129]. Additionally, Fink et al. fabricated an ultralong fiber supercapacitor by depositing a layer of activated carbon/polyvinylidene difluoride (PVDF) active material on the surface of copper wire using the hot-stretching technique (Fig. 9e). Benefiting from the high conductivity of copper wire, a 100-m-long fiber supercapacitor was successfully fabricated, which demonstrated exceptional washing performance (100 washing cycles) and mechanical strength (68 MPa) [130]. The fiber supercapacitor is not only capable of being woven manually into a 100 cm × 100 cm fabric but can also be modified for various situations using 3D printing technology. Combining graphene fibers with stretchy carboxylate polyurethane enables the self-healing capability of graphene fibers (Fig. 9f). The self-healing supercapacitor retained 82.4% of its capacitance after a 100% stretch and 54.2% of its capacitance after the third healing [131].

Continuous tuning of the components and structure of graphene fiber has led to a discernible enhancement in the electrochemical performance of fiber supercapacitors to date (Table 2). Meanwhile, its energy and power production capacity can be enhanced by connecting supercapacitors in series and parallel and employing nonwatery solid electrolyte. Consequently, the energy-consuming item has progressed from a single LED to an LED array and then to electronic display devices and intelligent sensing devices. In addition, by integrating the fiber capacitor with the energy generator, self-powered applications can be realized. Multiple core–shell porous graphene fibers were integrated into fiber supercapacitor chips by Qiu et al. to create a self-powered energy storage device using solar cells [99]. As depicted in Fig. 9g, the electric energy generated by the solar cells is first stored in the supercapacitor, and then, the supercapacitor drives the tiny walking robot to walk ~ 40 cm in 11.8 s, illustrating the commendable energy supply capacity of the fiber supercapacitor. Impressively, Wu et al. further incorporated nitrogen-doped graphene fiber into flexible fabric and built a simple intelligent wearable device based on this innovation [89]. As depicted in Fig. 9h, the assembled supercapacitor exhibited an energy density of 95.7 μWh/cm^2 and good flexibility to securely conform to the human body, thereby achieving a consistent energy source for portable music players, electronic displays, and watches. It is believed that due to the continuous optimization of fiber elements, fiber structure, and preparation process, the electromechanical and mechanical properties of fiber supercapacitors will be continuously enhanced to meet the needs of practical applications.

Flexible Energy Storage Applications for Fabric Supercapacitors

The fabric electrode woven from a single thread can effectively increase the area-specific capacitance of the electrode, resulting in a discernible rise in energy output capacity (Table 3). As depicted in Fig. 10a, the typical fabric supercapacitor consists of two fabric electrodes and one electrolyte layer. Carbon or copper film can also be used as a current collector to minimize the internal resistance of the supercapacitor. Similarly, the bending angle, bending radius, and device length can also be used as evaluation criteria for mechanical performance. In addition, as illustrated in Fig. 10b, commercial leather and fabric softness testers can assess the softness of fabric supercapacitors in accordance with ISO 17235 and the softness testing method for the leather or textile industries [128]. In the specific test procedure, a cylindrical rod of known quality is lowered at a predetermined rate to a set cloth. Softness (unit: mm) is defined as the distance between cylindrical rod protrusions that effectively reflects the softness of a fabric supercapacitor. A greater distance indicates that the supercapacitor is softer and therefore more comfortable to wear.

The fabric supercapacitor simultaneously demonstrates desirable electrochemical performance. Wu et al. integrated the anisotropic boron–carbon nanosheet fabric supercapacitors and commercial solar cells into a self-powered system, as depicted in Fig. 10c. After exposure to an environment approximating sunlight, the fabric supercapacitor drove the micro-lift successfully for 15 cycles, utilizing its advantages of large area and hierarchical structure [132]. On the contrary, the high energy output capabilities of the fabric supercapacitor make it simple to combine with diverse flexible display systems. As illustrated in Fig. 10d, a single fabric supercapacitor can successfully power a smart watch with 3 V output voltage and 15 mA output current [133]. Accordingly, multiple LED modules can be effectively powered by simply stitching it onto fabric [134]. By combining fabric supercapacitors with commercial battery soft packs, it is possible to increase the output voltage and current. As depicted in the right portion of Fig. 10d, it can offer an output voltage of 3.8 V and output current of 60 mA, which are sufficient to power a bigger color display screen.

The flexibility and high energy production capacity of the fabric electrode highlight its compatibility with intelligent wearable systems that often function under conditions of continuous motion (Fig. 10e) [140]. For instance, as represented in Fig. 10f, the fabric supercapacitor can provide

Table 2 Comparison of electrochemical performance of fiber supercapacitors

Material	Preparation methods	Electrolyte	Structure	$C_G/C_A/C_V$	Conductivity	Voltage	Energy density	Strength	Elongation	Stability	SSA
Porous graphene [61]	Wet spinning	1M H_2SO_4	Porous	409 F/g	2.5×10^3 S/m	0–1 V	14 Wh/kg	30 MPa	0.8%	5000	2605 m²/g
Hollow graphene [100]	Wet spinning	H_3PO_4/PVA	Interior porous structure	304.5 mF/cm²	4.8×10^3 S/m	0–0.8 V	27.1 µWh/cm²	631 MPa		10,000	71 m²/g
ST-GFs [103]	Drying spinning	H_2SO_4/PVA	Twist structure	973.1 mF/cm³	2.9×10^4 S/m	0–1 V	25.5 mWh/cm³	244 MPa	0.263%	10,000	
MXene/graphene [7]	Wet spinning	H_3PO_4/PVA	Heteroatom doping of graphene sheets	586.4 F/cm³	2.9×10^4 S/m	0–0.8 V	13.03 mWh/cm³	145 MPa	3.7%	3000	
Carbon polyhedrons/holey graphene [99]	Microfluidic spinning	H_3PO_4/PVA	Core–shell structure	2760 mF/cm²	1.3×10^4 S/m	0–0.8 V	335.8 mWh/cm²	306 MPa	2.8%	10,000	569 m²/g
N-doped MGFs [89]	Microfluidic spinning	H_3PO_4/PVA	Heteroatom doping of graphene sheets	1132 mF/cm²	3×10^4 S/m	0–0.8 V	95.7 µWh/cm²	90 MPa	4.2%	10,000	388 m²/g
Carbon black/graphene hybrid [110]	Wet spinning	H_3PO_4/PVA	Porous graphene	97.5 F/cm³	21.5 S/cm	0–1 V	1200 mW/cm³	159 MPa	14.5%	2000	254 m²/g
Porous sheath–core graphene [105]	Wet-spinning	H_2SO_4/PVA	Porous graphene	391.2 mF/cm²	4×10^3 S/m	0–0.8 V	8.7 mWh/cm²			7000	416 m²/g
Carbon nanotube/graphene [106]	Wet-spinning		Heteroatom doping of graphene sheets	62.1 F/cm³	28.2 S/cm	0–1 V	8.63 mWh/cm³	134 MPa	3.1%	20,000	268 m²/g
Wet-spun graphene films [111]	Wet-spinning	1 M H_2SO_4	Ordered structure	505 F/g		0–0.8 V		236 MPa	7.14%	10,000	158 m²/g
Molybdenum disulfide/reduced graphene [112]	Wet-spinning	H_3PO_4/PVA	Heteroatom doping of graphene sheets	134.38 F/g	3×10^4 S/m	0–1.2 V	32.24 mWh/cm³	109.44–204.27 MPa	14.2%	100	
Graphene Core-Sheath Microfibers [113]	Hydrothermal spinning	H_2SO_4/PVA	Core–shell structure	1.2 mF/cm²	1×10^3 S/m	0–0.8 V	0.17 µWh/cm²			500	
Single layered MoS_2/graphene [115]	Electrospinning	3 M KOH	Heteroatom doping of graphene sheets	334 F/g		− 1.0–0.2 V				5000	850 m²/g
d-MnO_2/holey graphene [116]	Wet-spinning	H_3PO_4/PVA	Porous graphene	16.3 mF/cm²		0–0.8 V		83 MPa		1000	107 m²/g
Tungsten nitride-coated graphene [119]	Wet-spinning	H_3PO_4/PVA	Heteroatom doping of graphene sheets	16.29 F/cm³	6×10^6 S/m	0–0.8 V	1.448 mWh/cm³	99 MPa		10,000	

Table 2 (continued)

Material	Preparation methods	Electrolyte	Structure	$C_G/C_A/C_V$	Conductivity	Voltage	Energy density	Strength	Elongation	Stability	SSA
Nanorod arrays/graphene [108]	Microfluidic spinning	H_3PO_4/PVA	Core–shell structure	230 mF/cm²	1.9×10^4 S/m	0–0.8 V	37.2 mWh/cm²			8000	
Nickel oxide arrays/graphene [120]	Microfluidic spinning	H_3PO_4/PVA	Core–shell structure	605.9 mF/cm²	1.7×10^4 S/m	0–0.8 V	120.3 µWh/cm²	122 MPa	3.83%	10,000	425 m²/g
Carbon nanotube–graphene [64]	Wet-spinning	H_3PO_4/PVA	Core–shell structure	300 F/cm²	1×10^4 S/m	0–1 V	6.3 mWh/cm³	84 MPa		1000	396 m²/g
Carbon fibers [129]	Wet spinning	H_3PO_4/PVA	Heteroatom doping of graphene sheets	243.9 mF/cm²	2.3×10^3 S/m	0–1.0 V	30.5 µWh/cm²			10,000	326 m²/g
Molybdenum oxide [8]	Controlled electrochemical oxidation	1 M NaCl	Ribbon structure	112.5 mF/cm²		0–1.0 V	15.64 mWh/cm²			2000	
Boron–Carbon Hetero [132]	Microfluidic electrospinning	$EMIBF_4$/PVDF-HFP	Heteroatom doping of graphene sheets	534.5 F/cm³	1.6×10^4 S/m	0–3.0 V	167 mWh/cm³			10,000	163 m²/g
Black phosphorous [133]	Microfluidic spinning	$EMIBF_4$/PVDF-HFP	Heteroatom doping of graphene sheets	308.7 F/cm³		0–3.0 V	96.5 mWh/cm³	313 MPa	17.96%	10,000	109 m²/g
Metal–organic framework/graphene/carbo [134]	Microliter droplet-based method	$EMIBF_4$	Heteroatom doping of graphene sheets	472 F/cm³	2.3×10^2 S/m	0–3.0 V	147.5 mWh/cm³			10,000	1206 m²/g
Black Phosphorus [135]	Droplet microfluidic strategy	2 M KOH	Ribbon structure	506 F/cm³		0–0.5 V	109.8 mWh/cm³			12,000	632 m²/g
Molybdenum Disulfide–Carbon Nanotubes [136]		2 M KOH	Ribbon structure	5485 F/g	1.1×10^6 S/m	0–0.6 V	226 mWh/g			8000	377 m²/g
ZnO NWs [137]	Hydrothermal spinning	1 M KNO_3	Ordered structure	0.21 mF/cm²	–	0–0.8 V	0.027 µWh/cm²	–	–	–	–
Porous gold/RuO_2 [34]	Microfluidic spinning	1 M H_2SO_4	Ordered structure	1220 mF/cm²	–	−0.3–0.7 V	7.9 mW/cm²	–	–	2000	–
GFSs [52]	Wet spinning	H_3PO_4/PVA	Layered structure	66.6 mF/cm²	3×10^4 S/m	0–1.0 V	–	–	–	5000	–
NG UCs [85]	Hydrothermal spinning	1 M $(C_2H_5)_4NBF_4$	Intrinsic layered structure	280 F/g	–	0–0.8 V	48 Wh/kg	–	–	10,000	–
MnO_2/GO [15]	Wet spinning	H_3PO_4/PVA	Hierarchically structure	66.1 F/cm³	2.5×10^3 S/m	0–0.8 V	5.8 mWh/cm³	117 MPa	–	10,000	139 m²/g

Table 2 (continued)

Material	Preparation methods	Electrolyte	Structure	$C_G/C_A/C_V$	Conductivity	Voltage	Energy density	Strength	Elongation	Stability	SSA
NS-GF [90]	Microfluidic spinning	1 M H_2SO_4	Porous structure	59.9 F/cm³	8.6×10^3 S/m	−0.4–0.6 V	8.3 mWh/cm²	74 MPa	–	10,000	312 m²/g
CP/HG FSCs [99]	Microfluidic spinning	H_3PO_4/PVA	Hierarchical structure	2760 mF/cm²	1.3×10^4 S/m	0–0.8 V	335.8 mWh/cm²	306 MPa	–	10,000	–
$Co_{1−x}S$/$CoFe_2O_4$@rGO [17]	Hydrothermal spinning	2 M KOH	Hierarchical-pore structure	2202 F/g	–	0–0.5 V	61.5 Wh/kg	–	–	20,000	–
PPy-MnO_2 nanoflakes-CF [5]	Wet spinning	H_3PO_4/PVA	Hybrid structure	69.3 F/cm³	–	0–0.8 V	0.04 W/cm³	–	–	1000	–
Graphene/MoS_2 [16]	Wet spinning	H_3PO_4/PVA	Hydrothermal structure	368 F/cm³	–	0–0.8 V	–	300 MPa	–	8000	–
r-PANI-GOF [18]	Wet spinning	H_2SO_4/PVA	Ordered structure	481 mF/cm²	–	0–0.8 V	42.76 µWh/cm²	–	–	5000	–
Cotton-RGO-AgNP [6]	Wet spinning	KOH/PVA	Ordered structure	12.09 mF/cm²	–	−1.0–0 V	100 µWh/cm³	–	–	10,000	–
HGHs [92]	Wet spinning	1 M H_2SO_4	Porous graphene`	283 F/g	2×10^3 S/m	0–1.0 V	77 Wh/kg	–	–	20,000	–
HGF [98]	Wet spinning	$EMIMBF_4$/AN	Porous structure	298 F/g	1×10^3 S/m	0–1.0 V	35 Wh/kg	–	–	20,000	–
CFs [94]	Wet spinning	–	Core–shell structure	–	0.8×10^6 S/m	−1.0–1.0 V	–	1.45 GPa	–	–	–
MXene-based fibers [7]	Wet spinning	2 M H_2SO_4	Ordered structure	586.4 F/cm³	2.9×10^4 S/m	0–0.8 V	13.03 mWh/cm³	145 MPa	–	3000	–
Hybrid fibres [64]	Hydrothermal spinning	2 M H_2SO_4	Porous structure	305 F/cm³	1×10^2 S/m	0–0.9 V	6.3 mWh/cm³	–	–	10,000	–

Table 3 Comparison of electrochemical performance of fabric supercapacitors

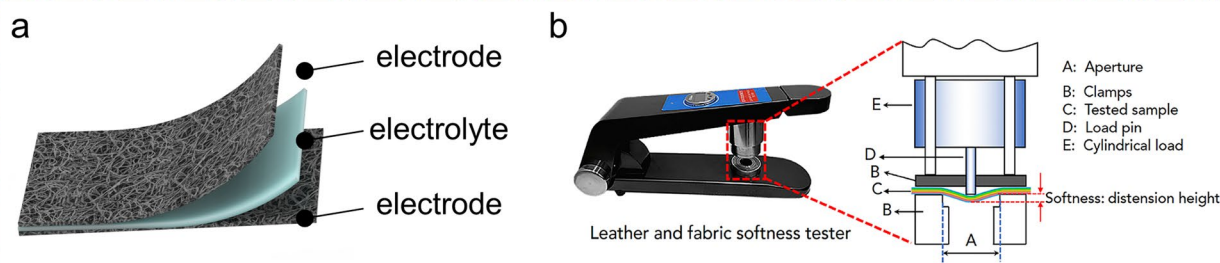| Material	Preparation methods	Electrolyte	Structure	$C_G/C_A/C_V$	Conductivity	Voltage	Energy density	Strength	Elongation	Stability	SSA
Carbonized cotton [138]	In situ electrodeposition	1 M Na_2SO_4	Heteroatom doping of graphene sheets	3596 mF/cm²		0–1.2 V	1.18 mWh/cm³			4000	
Graphene Fiber Fabrics [139]	Hydrothermal spinning	1 M H_2SO_4	Ordered structure	1060 mF/cm²		0–0.8 V	23.5 µWh/cm²			50,000	52 m²/g
Graphene Ribbons [101]	Wet spinning	2 M KCl	Ribbon structure	82.8 F/g	1.5×10^4 S/m	0–0.4 V	8.77 mW/cm²	100 MPa	14%	300	–
Graphene [121]	Screen-printing	6 M KOH	Heteroatom doping of graphene sheets	2695 mF/cm²		−1.0–0 V	147.6 mW/cm²			10,000	
Carbon fiber cloth [122]	Dip-coating	3 M HCl	Ordered structure	1421.6 F/g		0–1 V	589.7 W/kg			10,000	
TENG yarn [4]	Hydrothermal spinning	1 M KOH	Ordered structure	385.4 mF/cm²	1.1×10^6 S/m	−0.8–0 V	78.1 µWh/cm²	61.1 MPa	–	5000	–
GO [19]	Wet spinning	KOH	Hand woven	–	–	–	–	135 MPa	–	–	–
rGOFFs [20]	Wet spinning	1 M H_2SO_4	Ordered structure	285 F/g	1×10^3 S/m	0–1.0 V	28 µWh/cm²		–	10,000	–

energy for the pulse sensor and transmit the pulse signal back to the data coagulating terminal, thereby enabling the real-time monitoring of the heart rate during exercise. This is extremely important for personal health monitoring and individualized training plans for elite athletes [141]. In addition, as depicted in Fig. 10g, the fabric supercapacitor can easily power the temperature sensor under wide temperature changes (− 20–55 °C) [136]. Electrophysiological signals, biological posture signals, biological tissue dynamics signals, and biochemical signals can be monitored exhaustively by combining fabric capacitance with a variety of intelligent sensors [142].
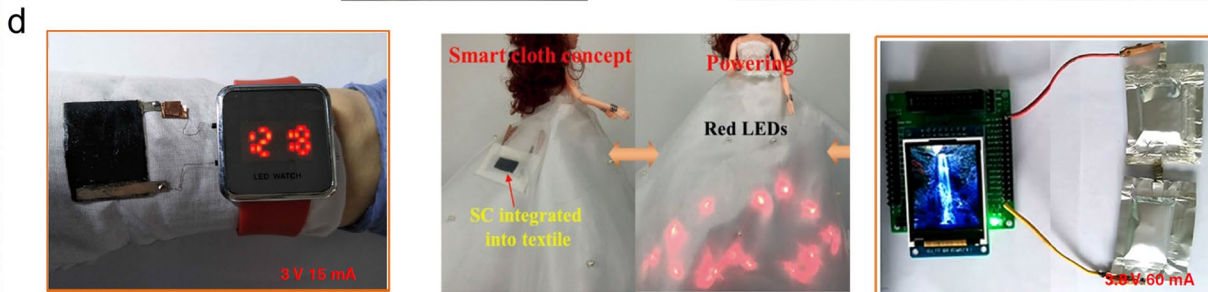
Summary and Outlook

Graphene fiber/fabric is a very competitive substrate for flexible electrodes with exceptional electrochemical and mechanical properties. Herein, the recent progress on graphene fiber/fabric-based supercapacitors is reviewed, focusing on the fabrication of graphene fiber elements, the control of fiber structure, and the preparation of fabrics. The relationship between fiber elements, fiber structure, and fabric preparation, in addition to their influence on the electrochemical and mechanical properties of supercapacitors, is explored.

To enhance the electrochemical activity, ion conductivity, and electrical conductivity of the fiber, it is crucial to control the chemical composition and structure of graphene sheets. For this, the shape and structure of fibers can be precisely manipulated by utilizing various spinning techniques, such as wet-spinning, restricted hydrothermal-spinning, and microfluid-spinning. By developing an appropriate fiber assembly process, vast quantities of graphene fiber/fabric can be produced to meet the practical application requirements of FSCs. Even though significant progress has been made in graphene fiber/fabric supercapacitors, there are still issues to be resolved before they can be utilized on a large scale. The following conclusions were drawn from this study:
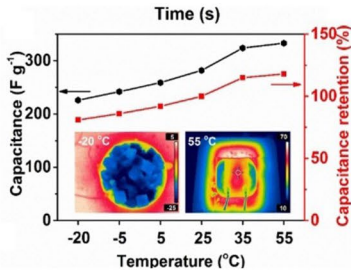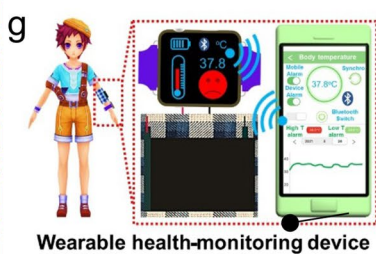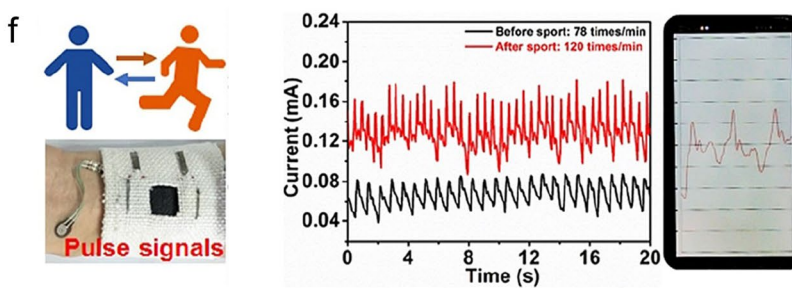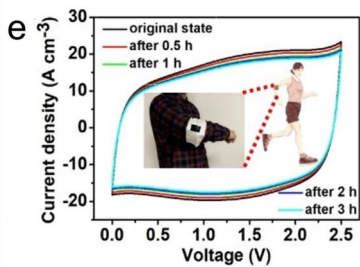
1. The restacking of graphene should be avoided as much as possible to maximize its particular surface area and quantum capacitance advantages. Even though numerous strategies have been devised to reduce the restacking impact of graphene, graphene fibers are still susceptible to partial restacking. In particular, the fiber electrode is anticipated to have excellent mechanical flexibility and conductivity as well as a porous structure, which places greater demands on the regulation of fiber elements and fiber preparation technology. In terms of graphene unit assembly, the production of large-sized graphene sheets with a porous structure is critical strategy. Pores

a

- electrode
- electrolyte
- electrode

b

E:
A: Aperture
B: Clamps
C: Tested sample
D: Load pin
E: Cylindrical load

Softness: distension height

Leather and fabric softness tester

The construction and mechanical characterization of fabrics supercapacitor

c

4 cm   10 cm

2 cm   + − × ÷ =   N J T U

Solar cell   FSC   Elevoter

Up   Up   Up   0 cm   5 cm   11 cm

d

LED WATCH   3 V 15 mA

Smart cloth concept   Powering   Red LEDs
SC integrated into textile

3.8 V 60 mA

Self power and Flexible display system

e

original state
after 0.5 h
after 1 h
after 2 h
after 3 h

Current density (A cm⁻³) vs Voltage (V)

f

Pulse signals

Before sport: 78 times/min
After sport: 120 times/min

Current (mA) vs Time (s)

g

Body temperature   37.8°C

Wearable health-monitoring device

Capacitance (F g⁻¹)   Capacitance retention (%)
Time (s)   Temperature (°C)
-20 °C   55 °C

Human skin surface temperature (T) monitoring   Low T alarm

Health monitoring system

in graphene sheets increase SSA and provide more ion adsorption sites and migration channels. Additionally, the larger size of graphene sheets improves the overall mechanical properties of the fiber. For fiber structure regulation, the inclusion of a barrier, freeze drying, and lamellar orientation modification have proven to be resulful for enhancing fiber porosity. This needs the adaptable and effective application of a range of spinning techniques.

2. New pseudocapacitance materials and in situ compounding approaches need to be developed. Due to their high electrochemical activity, pseudocapacitance materials have been extensively investigated since Conway et al. defined pseudocapacitance. However, in the practical use of graphene fiber/pseudocapacitance materials composites, issues such as peeling of pseudocapacitance materials, poor interface bonding between pseudocapacitance and graphene, and obstructed electron transport persist. The development of corresponding in situ composite technologies is a crucial strategy for addressing these issues. At the fiber element level, heteroatomic doping can increase the electrochemically active spots of graphene sheets and improve their conductivity. At the fiber structure level, chemical link between pseudocapacitance material and graphene sheet can substantially improve interface interaction and electron conduction by enhancing interface interaction. During spinning, an in situ chemical reaction can produce pseudocapacitive compounds directly between graphene lamellar layers. This could enhance interfacial electron conduction and prevent the spalling of pseudocapacitive materials as well as the lamellar restacking of graphene sheets. In this regard, developing new pseudocapacitance materials and enriching graphene fiber/pseudocapacitance composite system remains an essential area of study.

3. Further optimization of the current spinning technology and development of new spinning technology are required to produce fiber/fabric electrodes for large-scale practical applications. Scaling up the production of wet-spinning, restricted hydrothermal-spinning, microfluid-spinning, and blow-spinning methods is achievable. In addition, they entail a number of control factors, including temperature, coagulation bath, GO concentration, and spinning rate. Correspondingly, optimizing each parameter and understanding the preparation mechanism is crucial for large-scale production of graphene fibers/fabrics. In addition, the development of innovative graphene spinning techniques for improved fiber structure regulation should not be overlooked. Spinning graphene fibers primarily include (1) alignment of GO sheets in a limited region and (2) elimination of oxygen-containing functional groups. Due to the low solubility of graphene sheets relative to GO, step 1 is typically preceded by step 2, or both steps are performed simultaneously. Considering the relative importance of these two phases is beneficial for creating novel techniques for spinning graphene fibers.

4. Device-level research is still required to determine how to completely evaluate the performance of fiber/fabric supercapacitors. The electrochemical performance of a fiber/fabric supercapacitor can be quantified, including internal resistance, leakage current, output voltage, energy density, and power density [143]. However, few studies have been conducted on the mechanical flexibility and wearability of fiber/fabric supercapacitors. Existing reports mostly analyze the mechanical flexibility of devices based on the CV curve or capacity retention rate under various bending circumstances, which is insufficiently exhaustive. Therefore, more quantifiable performance indicators and testing methodologies should be designed to test flexible devices [144]. Simultaneously, it is necessary to monitor the change of electrochemical performance of the device under various test conditions for the iterative optimization of electrode materials.

5. Graphene fiber/fabric supercapacitor application systems must be investigated further. A mature, flexible, and wearable system contains numerous functional units, including an energy storage unit, sensing unit, energy generation unit (such as a friction generator or solar cell), and signal processing unit. Due to the complexity of the preparation procedure for graphene fiber/fabric capacitors, it is only now integrated with simple functional units such as LED, watch, and fan. Thus, to comprehensively evaluate the practical application performance of devices, more intelligent and practical wearable systems must be developed accordingly.

Data availability statement Data availability is not applicable to this article as no new data were created or analyzed in this article.

Declarations

Conflict of interest The authors state that there are no conflicts of interest to disclose.

References

1. Ray TR, Choi J, Bandodkar AJ, Krishnan S, Gutruf P, Tian L, Ghaffari R, Rogers JA. Bio-integrated wearable systems: a comprehensive review. *Chem Rev*. **2019**;*119*:5461.
2. Wang H, Zhang Y, Liang X, Zhang Y. Smart fibers and textiles for personal health management. *ACS Nano*. **2021**;*15*:12497.
3. Ma W, Zhang Y, Pan S, Cheng Y, Shao Z, Xiang H, Chen G, Zhu L, Weng W, Bai H, Zhu M. Smart fibers for energy conversion and storage. *Chem Soc Rev*. **2021**;*50*:7009.
4. Liu M, Cong Z, Pu X, Guo W, Liu T, Li M, Zhang Y, Hu W, Wang ZL. High-energy asymmetric supercapacitor yarns for self-charging power textiles. *Adv Funct Mater*. **2019**;*29*:1806298.
5. Tao J, Liu N, Ma W, Ding L, Li L, Su J, Gao Y. Solid-state high performance flexible supercapacitors based on polypyrrole-MnO2-carbon fiber hybrid structure. *Sci Rep*. **2013**;*3*:2286.
6. Xiao W, Huang J, Zhou W, Jiang Q, Deng Y, Zhang Y, Tian L. Surface modification of commercial cotton yarn as electrode for construction of flexible fiber-shaped supercapacitor. *Coatings*. **2021**;*11*:1086.
7. Yang QY, Xu Z, Fang B, Huang TQ, Cai SY, Chen H, Liu YJ, Gopalsamy K, Gao WW, Gao C. MXene/graphene hybrid fibers for high performance flexible supercapacitors. *J Mater Chem A*. **2017**;*5*:22113.
8. Sheng HW, Zhou JJ, Li B, He YH, Zhang XT, Liang J, Zhou JY, Su Q, Xie EQ, Lan W, Wang KR, Yu CJ. A thin, deformable, high-performance supercapacitor implant that can be biodegraded and bioabsorbed within an animal body. *Sci Adv*. **2021**;*7*:eabe3097.
9. Chen CR, Qin H, Cong HP, Yu SH. A highly stretchable and real-time healable supercapacitor. *Adv Mater*. **2019**;*31*: e1900573.
10. Gong W, Hou C, Zhou J, Guo Y, Zhang W, Li Y, Zhang Q, Wang H. Continuous and scalable manufacture of amphibious energy yarns and textiles. *Nat Commun*. **2019**;*10*:868.
11. Weng W, Yang J, Zhang Y, Li Y, Yang S, Zhu L, Zhu M. A route toward smart system integration: From fiber design to device construction. *Adv Mater*. **2020**;*32*:e1902301.
12. Geim AK. Graphene: status and prospects. *Science*. **2009**;*324*:1530.
13. Castro Neto AH, Guinea F, Peres NMR, Novoselov KS, Geim AK. The electronic properties of graphene. *Rev Mod Phys*. **2009**;*81*:109.
14. Ming X, Wei A, Liu Y, Peng L, Li P, Wang J, Liu S, Fang W, Wang Z, Peng H, Lin J, Huang H, Han Z, Luo S, Cao M, Wang B, Liu Z, Guo F, Xu Z, Gao C. 2d-topology-seeded graphitization for highly thermally conductive carbon fibers. *Adv Mater*. **2022**;*34*: e2201867.
15. Ma W, Chen S, Yang S, Chen W, Cheng Y, Guo Y, Peng S, Ramakrishna S, Zhu M. Hierarchical MnO2 nanowire/graphene hybrid fibers with excellent electrochemical performance for flexible solid-state supercapacitors. *J Power Sources*. **2016**;*306*:481.
16. Wang B, Wu Q, Sun H, Zhang J, Ren J, Luo Y, Wang M, Peng H. An intercalated graphene/(molybdenum disulfide) hybrid fiber for capacitive energy storage. *J Mater Chem A*. **2017**;*5*:925.
17. Ren C, Jia X, Zhang W, Hou D, Xia Z, Huang D, Hu J, Chen S, Gao S. Hierarchical porous integrated co$_{1-x}$s/cofe$_2$o$_4$@rgo nano-flowers fabricated via temperature-controlled in situ calcining sulfurization of multivariate cofe-mof-74@rgo for high-performance supercapacitor. *Adv Funct Mater*. **2020**;*30*:2004519.
18. Wu Y, Meng Z, Yang J, Xue Y. Flexible fiber-shaped supercapacitors based on graphene/polyaniline hybrid fibers with high energy density and capacitance. *Nanotechnology*. **2021**;*32*: 295401.
19. Seyedin S, Romano MS, Minett AI, Razal JM. Towards the knittability of graphene oxide fibres. *Sci Rep*. **2015**;*5*:14946.
20. Shao F, Hu N, Su Y, Yao L, Li B, Zou C, Li G, Zhang C, Li H, Yang Z, Zhang Y. Non-woven fabric electrodes based on graphene-based fibers for areal-energy-dense flexible solid-state supercapacitors. *Chem Eng J*. **2020**;*392*: 123692.
21. Fang B, Chang D, Xu Z, Gao C. A review on graphene fibers: Expectations, advances, and prospects. *Adv Mater*. **2020**;*32*: e1902664.
22. Xu T, Zhang Z, Qu L. Graphene-based fibers: recent advances in preparation and application. *Adv Mater*. **2020**;*32*: e1901979.
23. Zhang Y, Ding J, Qi B, Tao W, Wang J, Zhao C, Peng H, Shi J. Multifunctional fibers to shape future biomedical devices. *Adv Funct Mater*. **2019**;*29*:1902834.
24. Ding J, Hu W, Paek E, Mitlin D. Review of hybrid ion capacitors: from aqueous to lithium to sodium. *Chem Rev*. **2018**;*118*:6457.
25. Grahame DC. The electrical double layer and the theory of electrocapillarity. *Chem Rev*. **1947**;*41*:441.
26. Chmiola J, Yushin G, Gogotsi Y, Portet C, Simon P, Taberna PL. Anomalous increase in carbon capacitance at pore sizes less than 1 nanometer. *Science*. **2006**;*313*:1760.
27. Liu YM, Merlet C, Smit B. Carbons with regular pore geometry yield fundamental insights into supercapacitor charge storage. *ACS Central Sci*. **1813**;*2019*:5.
28. Ji H, Zhao X, Qiao Z, Jung J, Zhu Y, Lu Y, Zhang LL, MacDonald AH, Ruoff RS. Capacitance of carbon-based electrical double-layer capacitors. *Nat Commun*. **2014**;*5*:3317.
29. Choi C, Ashby DS, Butts DM, DeBlock RH, Wei Q, Lau J, Dunn B. Achieving high energy density and high power density with pseudocapacitive materials. *Nat Rev Mater*. **2019**;*5*:5.
30. Augustyn V, Come J, Lowe MA, Kim JW, Taberna PL, Tolbert SH, Abruna HD, Simon P, Dunn B. High-rate electrochemical energy storage through Li$^+$ intercalation pseudocapacitance. *Nat Mater*. **2013**;*12*:518.
31. Lukatskaya MR, Mashtalir O, Ren CE, Dall'Agnese Y, Rozier P, Taberna PL, Naguib M, Simon P, Barsoum MW, Gogotsi Y. Cation intercalation and high volumetric capacitance of two-dimensional titanium carbide. *Science*. **2013**;*341*:1502.
32. Simon P, Gogotsi Y. Perspectives for electrochemical capacitors and related devices. *Nat Mater*. **2020**;*19*:1151.
33. Lee HY, Goodenough JB. Supercapacitor behavior with KCl electrolyte. *J Solid State Chem*. **1999**;*144*:220.
34. Ferris A, Garbarino S, Guay D, Pech D. 3d RuO2 microsupercapacitors with remarkable areal energy. *Adv Mater*. **2015**;*27*:6625.
35. Berggren M, Malliaras GG. How conducting polymer electrodes operate. *Science*. **2019**;*364*:233.
36. Jiang Y, Liu J. Definitions of pseudocapacitive materials: a brief review. *Energy Environ Mater*. **2019**;*2*:30.
37. Pu X, Zhao D, Fu C, Chen Z, Cao S, Wang C, Cao Y. Understanding and calibration of charge storage mechanism in cyclic voltammetry curves. *Angew Chem Int Ed*. **2021**;*60*:21310.
38. Zuo W, Li R, Zhou C, Li Y, Xia J, Liu J. Battery-supercapacitor hybrid devices: recent progress and future prospects. *Adv Sci*. **2017**;*4*:1600539.

39. Chatterjee DP, Nandi AK. A review on the recent advances in hybrid supercapacitors. *J Mater Chem A*. **2021**;*9*:15880.

40. Chen S, Qiu L, Cheng HM. Carbon-based fibers for advanced electrochemical energy storage devices. *Chem Rev*. **2020**;*120*:2811.

41. Lin L, Peng H, Liu Z. Synthesis challenges for graphene industry. *Nat Mater*. **2019**;*18*:520.

42. Xu Y, Sheng K, Li C, Shi G. Highly conductive chemically converted graphene prepared from mildly oxidized graphene oxide. *J Mater Chem A*. **2011**;*21*:7376.

43. Eigler S, Hirsch A. Chemistry with graphene and graphene oxide-challenges for synthetic chemists. *Angew Chem Int Ed*. **2014**;*53*:7720.

44. Li C, Lin J, Shen L, Bao N. Quantitative analysis and kinetic modeling of ultrasound-assisted exfoliation and breakage process of graphite oxide. *Chem Eng Sci*. **2020**;*213*: 115414.

45. Chen J, Li Y, Huang L, Jia N, Li C, Shi G. Size fractionation of graphene oxide sheets via filtration through track-etched membranes. *Adv Mater*. **2015**;*27*:3654.

46. Weng C, Wu J, Shen L, Bao N. Shear exfoliation of large-size GO sheets for high-performance films. *J Mater Sci*. **2021**;*56*:18946.

47. Kang JH, Kim T, Choi J, Park J, Kim YS, Chang MS, Jung H, Park KT, Yang SJ, Park CR. Hidden second oxidation step of hummers method. *Chem Mater*. **2016**;*28*:756.

48. Li C, Guo Y, Shen L, Ji C, Bao N. Scalable concentration process of graphene oxide dispersions via cross-flow membrane filtration. *Chem Eng Sci*. **2019**;*200*:127.

49. Wang RH, Wang Y, Xu CH, Sun J, Gao L. Facile one-step hydrazine-assisted solvothermal synthesis of nitrogen-doped reduced graphene oxide: reduction effect and mechanisms. *Rsc Adv*. **2013**;*3*:1194.

50. Ren PG, Yan DX, Ji X, Chen T, Li ZM. Temperature dependence of graphene oxide reduced by hydrazine hydrate. *Nanotechnology*. **2011**;*22*: 055705.

51. Pei SF, Zhao JP, Du JH, Ren WC, Cheng HM. Direct reduction of graphene oxide films into highly conductive and flexible graphene films by hydrohalic acids. *Carbon*. **2010**;*48*:4466.

52. Huang T, Zheng B, Kou L, Gopalsamy K, Xu Z, Gao C, Meng Y, Wei Z. Flexible high performance wet-spun graphene fiber supercapacitors. *RSC Adv*. **2013**;*3*:23957.

53. Jung I, Field DA, Clark NJ, Zhu YW, Yang DX, Piner RD, Stankovich S, Dikin DA, Geisler H, Ventrice CA, Ruoff RS. Reduction kinetics of graphene oxide determined by electrical transport measurements and temperature programmed desorption. *J Phys Chem C*. **2009**;*113*:18480.

54. Yin KB, Li HT, Xia YD, Bi HC, Sun J, Liu ZG, Sun LT. Thermodynamic and kinetic analysis of low-temperature thermal reduction of graphene oxide. *Nano-Micro Lett*. **2011**;*3*:51.

55. Xu Z, Gao C. Graphene chiral liquid crystals and macroscopic assembled fibres. *Nat Commun*. **2011**;*2*:571.

56. Xu Z, Peng L, Liu Y, Liu Z, Sun H, Gao W, Gao C. Experimental guidance to graphene macroscopic wet-spun fibers, continuous papers, and ultralightweight aerogels. *Chem Mater*. **2016**;*29*:319.

57. Xu Z, Sun H, Zhao X, Gao C. Ultrastrong fibers assembled from giant graphene oxide sheets. *Adv Mater*. **2013**;*25*:188.

58. Shim YH, Ahn H, Lee S, Kim SO, Kim SY. Universal alignment of graphene oxide in suspensions and fibers. *ACS Nano*. **2021**;*15*:13453.

59. Cao J, Zhang Y, Men C, Sun Y, Wang Z, Zhang X, Li Q. Programmable writing of graphene oxide/reduced graphene oxide fibers for sensible networks with in situ welded junctions. *ACS Nano*. **2014**;*8*:4325.

60. Wu C, Wang X, Zhuo Q, Sun J, Qin C, Wang J, Dai L. A facile continuous wet-spinning of graphene oxide fibers from aqueous solutions at high pH with the introduction of ammonia. *Carbon*. **2018**;*138*:292.

61. Aboutalebi SH, Jalili R, Esrafilzadeh D, Salari M, Gholamvand Z, Aminorroaya Yamini S, Konstantinov K, Shepherd RL, Chen J, Moulton SE, Innis PC, Minett AI, Razal JM, Wallace GG. High-performance multifunctional graphene yarns: toward wearable all-carbon energy storage textiles. *ACS Nano*. **2014**;*8*:2456.

62. Liao M, Sun H, Zhang J, Wu J, Xie S, Fu X, Sun X, Wang B, Peng H. Multicolor, fluorescent supercapacitor fiber. *Small*. **2018**;*14*: e1702052.

63. Cruz-Silva R, Morelos-Gomez A, Kim HI, Jang HK, Tristan F, Vega-Diaz S, Rajukumar LP, Elias AL, Perea-Lopez N, Suhr J, Endo M, Terrones M. Super-stretchable graphene oxide macroscopic fibers with outstanding knotability fabricated by dry film scrolling. *ACS Nano*. **2014**;*8*:5959.

64. Yu D, Goh K, Wang H, Wei L, Jiang W, Zhang Q, Dai L, Chen Y. Scalable synthesis of hierarchically structured carbon nanotube-graphene fibres for capacitive energy storage. *Nat Nanotechnol*. **2014**;*9*:555.

65. Ma P, Li P, Wang Y, Chang D, Gao WW, Gao C. Liquid crystal-line microdroplets of graphene oxide via microfluidics. *Chinese J Polym Sci*. **2021**;*39*:1657.

66. Hu X, Tian M, Pan N, Sun B, Li Z, Ma Y, Zhang X, Zhu S, Chen Z, Qu L. Structure-tunable graphene oxide fibers via microfluidic spinning route for multifunctional textiles. *Carbon*. **2019**;*152*:106.

67. Tian Q, Xu Z, Liu Y, Fang B, Peng L, Xi J, Li Z, Gao C. Dry spinning approach to continuous graphene fibers with high toughness. *Nanoscale*. **2017**;*9*:12335.

68. Zhang ZF, Zhang P, Zhang DS, Lin H, Chen YY. A new strategy for the preparation of flexible macroscopic graphene fibers as supercapacitor electrodes. *Mater Design*. **2018**;*157*:170.

69. Hua C, Shang Y, Li X, Hu X, Wang Y, Wang X, Zhang Y, Li X, Duan H, Cao A. Helical graphene oxide fibers as a stretchable sensor and an electrocapillary sucker. *Nanoscale*. **2016**;*8*:10659.

70. Nardecchia S, Carriazo D, Ferrer ML, Gutierrez MC, del Monte F. Three dimensional macroporous architectures and aerogels built of carbon nanotubes and/or graphene: synthesis and applications. *Chem Soc Rev*. **2013**;*42*:794.

71. Dong Z, Jiang C, Cheng H, Zhao Y, Shi G, Jiang L, Qu L. Facile fabrication of light, flexible and multifunctional graphene fibers. *Adv Mater*. **1856**;*2012*:24.

72. Du XY, Li Q, Wu G, Chen S. Multifunctional micro/nanoscale fibers based on microfluidic spinning technology. *Adv Mater*. **2019**;*31*: e1903733.

73. Xin G, Zhu W, Deng Y, Cheng J, Zhang LT, Chung AJ, De S, Lian J. Microfluidics-enabled orientation and microstructure control of macroscopic graphene fibres. *Nat Nanotechnol*. **2019**;*14*:168.

74. Rocha JF, Hostert L, Bejarano MLM, Cardoso RM, Santos MD, Maroneze CM, Gongora-Rubio MR, Silva CCC. Graphene oxide fibers by microfluidics assembly: a strategy for structural and dimensional control. *Nanoscale*. **2021**;*13*:6752.

75. Liu H, Zhou F, Shi X, Shi Q, Wu Z-S. Recent advances and prospects of graphene-based fibers for application in energy storage devices. *Acta Phys Chim Sin*. **2022**;*0*:2204017.

76. Yao W, Liu H, Sun J, Wu B, Liu Y. Engineering of chemical vapor deposition graphene layers: growth, characterization, and properties. *Adv Funct Mater*. **2022**;*32*:2202584.

77. Wu P, Zhang W, Li Z, Yang J. Mechanisms of graphene growth on metal surfaces: theoretical perspectives. *Small*. **2014**;*10*:2136.

78. Li X, Zhao T, Wang K, Yang Y, Wei J, Kang F, Wu D, Zhu H. Directly drawing self-assembled, porous, and monolithic graphene fiber from chemical vapor deposition grown graphene film and its electrochemical properties. *Langmuir*. **2011**;*27*:12164.

79. Chen T, Dai L. Macroscopic graphene fibers directly assembled from cvd-grown fiber-shaped hollow graphene tubes. *Angew Chem Int Ed*. **2015**;*54*:14947.

80. Chen K, Zhou X, Cheng X, Qiao R, Cheng Y, Liu C, Xie Y, Yu W, Yao F, Sun Z, Wang F, Liu K, Liu Z. Graphene photonic crystal fibre with strong and tunable light–matter interaction. *Nat Photonics*. **2019**;*13*:754.

81. Jian M, Zhang Y, Liu Z. Graphene fibers: preparation, properties, and applications. *Acta Physico Chimica Sinica*. **2020**;*38*:2007093.

82. Guan TX, Shen LM, Bao NZ. Hydrophilicity improvement of graphene fibers for high-performance flexible supercapacitor. *Ind Eng Chem Res*. **2019**;*58*:17338.

83. Wang X, Sun G, Routh P, Kim DH, Huang W, Chen P. Heteroatom-doped graphene materials: syntheses, properties and applications. *Chem Soc Rev*. **2014**;*43*:7067.

84. Xue Y, Wu B, Bao Q, Liu Y. Controllable synthesis of doped graphene and its applications. *Small*. **2014**;*10*:2975.

85. Jeong HM, Lee JW, Shin WH, Choi YJ, Shin HJ, Kang JK, Choi JW. Nitrogen-doped graphene for high-performance ultra-capacitors and the importance of nitrogen-doped sites at basal planes. *Nano Lett*. **2011**;*11*:2472.

86. Jeon IY, Choi HJ, Ju MJ, Choi IT, Lim K, Ko J, Kim HK, Kim JC, Lee JJ, Shin D, Jung SM, Seo JM, Kim MJ, Park N, Dai L, Baek JB. Direct nitrogen fixation at the edges of graphene nanoplatelets as efficient electrocatalysts for energy conversion. *Sci Rep*. **2013**;*3*:2260.

87. Wu ZS, Ren WC, Xu L, Li F, Cheng HM. Doped graphene sheets as anode materials with superhigh rate and large capacity for lithium ion batteries. *ACS Nano*. **2011**;*5*:5463.

88. Wu P, Cai Z, Gao Y, Zhang H, Cai C. Enhancing the electrochemical reduction of hydrogen peroxide based on nitrogen-doped graphene for measurement of its releasing process from living cells. *Chem Commun*. **2011**;*47*:11327.

89. Wu G, Tan P, Wu X, Peng L, Cheng H, Wang CF, Chen W, Yu Z, Chen S. High-performance wearable micro-supercapacitors based on microfluidic-directed nitrogen-doped graphene fiber electrodes. *Adv Funct Mater*. **2017**;*27*:1702493.

90. Ma W, Li W, Li M, Mao Q, Pan Z, Zhu M, Zhang Y. Scalable microgel spinning of a three-dimensional porous graphene fiber for high-performance flexible supercapacitors. *J Mater Chem A*. **2020**;*8*:25355.

91. Zhao T, Yang D, Xu T, Zhang M, Zhang S, Qin L, Yu ZZ. Cold-resistant nitrogen/sulfur dual-doped graphene fiber supercapacitors with solar-thermal energy conversion effect. *Chemistry*. **2021**;*27*:3473.

92. Xu Y, Chen CY, Zhao Z, Lin Z, Lee C, Xu X, Wang C, Huang Y, Shakir MI, Duan X. Solution processable holey graphene oxide and its derived macrostructures for high-performance supercapacitors. *Nano Lett*. **2015**;*15*:4605.

93. Zhu Y, Murali S, Stoller MD, Ganesh KJ, Cai W, Ferreira PJ, Pirkle A, Wallace RM, Cychosz KA, Thommes M, Su D, Stach EA, Ruoff RS. Carbon-based supercapacitors produced by activation of graphene. *Science*. **2011**;*332*:1537.

94. Xu Z, Liu Y, Zhao X, Peng L, Sun H, Xu Y, Ren X, Jin C, Xu P, Wang M, Gao C. Ultrastiff and strong graphene fibers via full-scale synergetic defect engineering. *Adv Mater*. **2016**;*28*:6449.

95. Cheng Y, Cui G, Liu C, Liu Z, Yan L, Liu B, Yuan H, Shi P, Jiang J, Huang K, Wang K, Cheng S, Li J, Gao P, Zhang X, Qi Y, Liu Z. Electric current aligning component units during graphene fiber joule heating. *Adv Funct Mater*. **2021**;*32*:2103493.

96. Guan TX, Shen S, Cheng ZS, Wu G, Bao NZ. Microfluidic-assembled hierarchical macro-microporous graphene fabrics towards high-performance robust supercapacitors. *Chem Eng J*. **2022**;*440*: 135878.

97. Radich EJ, Kamat PV. Making graphene holey. Gold-nanoparticle-mediated hydroxyl radical attack on reduced graphene oxide. *ACS Nano*. **2013**;*7*:5546.

98. Xu Y, Lin Z, Zhong X, Huang X, Weiss NO, Huang Y, Duan X. Holey graphene frameworks for highly efficient capacitive energy storage. *Nat Commun*. **2014**;*5*:4554.

99. Qiu H, Cheng H, Meng J, Wu G, Chen S. Magnetothermal microfluidic-assisted hierarchical microfibers for ultra-high-energy-density supercapacitors. *Angew Chem Int Ed*. **2020**;*59*:7934.

100. Qu G, Cheng J, Li X, Yuan D, Chen P, Chen X, Wang B, Peng H. A fiber supercapacitor with high energy density based on hollow graphene/conducting polymer fiber electrode. *Adv Mater*. **2016**;*28*:3646.

101. Sun J, Li Y, Peng Q, Hou S, Zou D, Shang Y, Li Y, Li P, Du Q, Wang Z, Xia Y, Xia L, Li X, Cao A. Macroscopic, flexible, high-performance graphene ribbons. *ACS Nano*. **2013**;*7*:10225.

102. Xiang X, Yang Z, Di J, Zhang W, Li R, Kang L, Zhang Y, Zhang H, Li Q. In situ twisting for stabilizing and toughening conductive graphene yarns. *Nanoscale*. **2017**;*9*:11523.

103. Zhang ZF, Zhang DS, Lin H, Chen YY. Flexible fiber-shaped supercapacitors with high energy density based on self-twisted graphene fibers. *J Power Sources*. **2019**;*433*: 226711.

104. Fang B, Xiao Y, Xu Z, Chang D, Wang B, Gao W, Gao C. Handedness-controlled and solvent-driven actuators with twisted fibers. *Mater Horiz*. **2019**;*6*:1207.

105. Zheng X, Zhang K, Yao L, Qiu Y, Wang S. Hierarchically porous sheath–core graphene-based fiber-shaped supercapacitors with high energy density. *J Mater Chem A*. **2018**;*6*:896.

106. Ma W, Li W, Li M, Mao Q, Pan Z, Hu J, Li X, Zhu M, Zhang Y. Unzipped carbon nanotube/graphene hybrid fiber with less "dead volume" for ultrahigh volumetric energy density supercapacitors. *Adv Funct Mater*. **2021**;*31*:2100195.

107. Guan T, Cheng Z, Li Z, Gao L, Yan K, Shen L, Bao N. Hydrothermal-assisted in situ growth of vertically aligned MoS2 nanosheets on reduced graphene oxide fiber fabrics toward high-performance flexible supercapacitors. *Ind Eng Chem Res*. **2022**;*61*:3840.

108. Wu X, Wu G, Tan P, Cheng H, Hong R, Wang F, Chen S. Construction of microfluidic-oriented polyaniline nanorod arrays/graphene composite fibers for application in wearable micro-supercapacitors. *J Mater Chem A*. **2018**;*6*:8940.

109. Miller JR, Outlaw RA, Holloway BC. Graphene double-layer capacitor with ac line-filtering performance. *Science*. **2010**;*329*:1637.

110. Ma WJ, Chen SH, Yang SY, Zhu MF. Hierarchically porous carbon black/graphene hybrid fibers for high performance flexible supercapacitors. *Rsc Adv*. **2016**;*6*:50112.

111. Huang T, Zheng B, Liu Z, Kou L, Gao C. High rate capability supercapacitors assembled from wet-spun graphene films with a CaCO₃ template. *J Mater Chem A*. **1890**;*2015*:3.

112. Li J, Shao Y, Jiang P, Zhang Q, Hou C, Li Y, Wang H. 1T-Molybdenum disulfide/reduced graphene oxide hybrid fibers as high strength fibrous electrodes for wearable energy storage. *J Mater Chem A*. **2019**;*7*:3143.

113. Meng Y, Zhao Y, Hu C, Cheng H, Hu Y, Zhang Z, Shi G, Qu L. All-graphene core-sheath microfibers for all-solid-state, stretchable fibriform supercapacitors and wearable electronic textiles. *Adv Mater*. **2013**;*25*:2326.

114. Hu WX, Xiang RF, Zhang K, Xu QL, Liu Y, Jing YY, Zhang J, Hu XF, Zheng YY, Jin YH, Yang XN, Lu CH. Electrochemical performance of coaxially wet-spun hierarchically porous lignin-based carbon/graphene fiber electrodes for flexible supercapacitors. *Acs Appl Energ Mater*. **2021**;*4*:9077.

115. Fu H, Zhang X, Fu J, Shen G, Ding Y, Chen Z, Du H. Single layers of MoS2/Graphene nanosheets embedded in activated carbon nanofibers for high-performance supercapacitor. *J Alloy Compd*. **2020**;*829*: 154557.

116. Zhang J, Yang X, He Y, Bai Y, Kang L, Xu H, Shi F, Lei Z, Liu Z-H. δ-MnO₂/holey graphene hybrid fiber for all-solid-state supercapacitor. *J Mater Chem A*. **2016**;*4*:9088.

117. Yang J, Weng W, Liang Y, Zhang Y, Yang L, Luo X, Liu Q, Zhu M. Heterogeneous graphene/polypyrrole multilayered microtube with enhanced capacitance. *Electrochim Acta*. **2019**;*304*:378.

118. Cai S, Huang T, Chen H, Salman M, Gopalsamy K, Gao C. Wet-spinning of ternary synergistic coaxial fibers for high performance yarn supercapacitors. *J Mater Chem A*. **2017**;*5*:22489.

119. Salman A, Padmajan Sasikala S, Kim IH, Kim JT, Lee GS, Kim JG, Kim SO. Tungsten nitride-coated graphene fibers for high-performance wearable supercapacitors. *Nanoscale*. **2020**;*12*:20239.

120. Meng J, Wu G, Wu X, Cheng H, Xu Z, Chen S. Microfluidic-architected nanoarrays/porous core-shell fibers toward robust micro-energy-storage. *Adv Sci*. **2020**;*7*:1901931.

121. Keawploy N, Venkatkarthick R, Wangyao P, Zhang X, Liu R, Qin J. Eco-friendly conductive cotton-based textile electrodes using silver- and carbon-coated fabrics for advanced flexible supercapacitors. *Energ Fuel*. **2020**;*34*:8977.

122. Wu Z, Jiang L, Tian W, Wang Y, Jiang Y, Gu Q, Hu L. Novel sub-5 nm layered niobium phosphate nanosheets for high-voltage, cation-intercalation typed electrochemical energy storage in wearable pseudocapacitors. *Adv Energy Mater*. **2019**;*9*:1900111.

123. Liu Z, Zhang X, Liu C, Li D, Zhang M, Yin F, Xin G, Wang G. Ferroconcrete-inspired design of a nonwoven graphene fiber fabric reinforced electrode for flexible fast-charging sodium ion storage devices. *J Mater Chem A*. **2020**;*8*:2777.

124. Chang D, Liu J, Fang B, Xu Z, Li Z, Liu Y, Brassart L, Guo F, Gao W, Gao C. Reversible fusion and fission of graphene oxide–based fibers. *Science*. **2021**;*372*:614.

125. Li Z, Xu Z, Liu Y, Wang R, Gao C. Multifunctional non-woven fabrics of interfused graphene fibres. *Nat Commun*. **2016**;*7*:13684.

126. Liu S, Wang Y, Ming X, Xu Z, Liu Y, Gao C. High-speed blow spinning of neat graphene fibrous materials. *Nano Lett*. **2021**;*21*:5116.

127. Le VT, Kim H, Ghosh A, Kim J, Chang J, Vu QA, Pham DT, Lee JH, Kim SW, Lee YH. Coaxial fiber supercapacitor using all-carbon material electrodes. *ACS Nano*. **2013**;*7*:5940.

128. Li H, Tang Z, Liu Z, Zhi C. Evaluating flexibility and wearability of flexible energy storage devices. *Joule*. **2019**;*3*:613.

129. Lee YG, Lee J, An GH. Surface engineering of carbon via coupled porosity tuning and heteroatom-doping for high-performance flexible fibrous supercapacitors. *Adv Funct Mater*. **2021**;*31*:2104256.

130. Khudiyev T, Lee JT, Cox JR, Argentieri E, Loke G, Yuan R, Noel GH, Tatara R, Yu Y, Logan F, Joannopoulos J, Shao-Horn Y, Fink Y. 100 m long thermally drawn supercapacitor fibers with applications to 3d printing and textiles. *Adv Mater*. **2020**;*32*: e2004971.

131. Wang S, Liu N, Su J, Li L, Long F, Zou Z, Jiang X, Gao Y. Highly stretchable and self-healable supercapacitor with reduced graphene oxide based fiber springs. *ACS Nano*. **2017**;*11*:2066.

132. Wu T, Wu X, Li L, Hao M, Wu G, Zhang T, Chen S. Anisotropic boron-carbon hetero-nanosheets for ultrahigh energy density supercapacitors. *Angew Chem Int Ed*. **2020**;*59*:23800.

133. Wu X, Xu Y, Hu Y, Wu G, Cheng H, Yu Q, Zhang K, Chen W, Chen S. Microfluidic-spinning construction of black-phosphorus-hybrid microfibres for non-woven fabrics toward a high energy density flexible supercapacitor. *Nat Commun*. **2018**;*9*:4573.

134. Cheng H, Meng J, Wu G, Chen S. Hierarchical micro-mesoporous carbon-framework-based hybrid nanofibres for high-density capacitive energy storage. *Angew Chem Int Ed*. **2019**;*58*:17465.

135. Wu T, Ma Z, He Y, Wu X, Tang B, Yu Z, Wu G, Chen S, Bao N. A Covalent Black Phosphorus/Metal-Organic Framework Hetero-nanostructure for High-Performance Flexible Supercapacitors. *Angew Chem Int Ed*. **2021**;*60*:10366.

136. Wu X, Zhu X, Tao H, Wu G, Xu J, Bao N. Covalently aligned molybdenum disulfide-carbon nanotubes heteroarchitecture for high-performance electrochemical capacitors. *Angew Chem Int Ed*. **2021**;*60*:21295.

137. Bae J, Song MK, Park YJ, Kim JM, Liu M, Wang ZL. Fiber supercapacitors made of nanowire-fiber hybrid structures for wearable/flexible energy storage. *Angew Chem Int Ed*. **2011**;*50*:1683.

138. Sun C, Li X, Cai ZS, Ge FY. Carbonized cotton fabric in-situ electrodeposition polypyrrole as high-performance flexible electrode for wearable supercapacitor. *Electrochim Acta*. **2019**;*296*:617.

139. Li Z, Huang T, Gao W, Xu Z, Chang D, Zhang C, Gao C. Hydrothermally activated graphene fiber fabrics for textile electrodes of supercapacitors. *ACS Nano*. **2017**;*11*:11056.

140. Wu T, Ma Z, He Y, Wu X, Tang B, Yu Z, Wu G, Chen S, Bao N. A covalent black phosphorus/metal–organic framework hetero-nanostructure for high-performance flexible supercapacitors. *Angew Chem Int Edit*. **2021**;*60*:10366.

141. Su B, Li J, Xu H, Xu Z, Meng J, Chen X, Li F. Scientific athletics training: flexible sensors and wearable devices forkineses monitoring applications. *Scientia Sinica Informationis*. **2022**;*52*:54.

142. Jang Y, Kim SM, Spinks GM, Kim SJ. Carbon nanotube yarn for fiber-shaped electrical sensors, actuators, and energy storage for smart systems. *Adv Mater*. **2020**;*32*: e1902670.

143. Shao Y, El-Kady MF, Sun J, Li Y, Zhang Q, Zhu M, Wang H, Dunn B, Kaner RB. Design and mechanisms of asymmetric supercapacitors. *Chem Rev*. **2018**;*118*:9233.

144. He J, Lu C, Jiang H, Han F, Shi X, Wu J, Wang L, Chen T, Wang J, Zhang Y, Yang H, Zhang G, Sun X, Wang B, Chen P, Wang Y, Xia Y, Peng H. Scalable production of high-performing woven lithium-ion fibre batteries. *Nature*. **2021**;*597*:57.

Tuxiang Guan received his Ph.D. in chemical engineering from Nanjing Tech University, China, in 2022. He is a postdoctor in the College of Chemical Engineering at Nanjing Tech University. His research interest includes 2D nanomaterials, flexible supercapacitors/battery and wearable applications.

Meifang Zhu obtained her Ph.D. on Materials Science in 1999 from Donghua University (DHU, Shanghai). Currently, she is a professor at DHU and the member of Chinese Academy of Science. She also serves as the dean for the College of Materials Science and Engineering in DHU, and the director of the State Key Laboratory for Modification of Chemical Fibers and Polymer Materials. She has long been engaged in fundamental chemistry, properties, and applications research of fiber materials, organic/inorganic hybrid nano-materials, smart hydrogels and biomaterials for green energy, environment, and healthcare.

Ningzhong Bao received his Ph.D. in chemical engineering from Nanjing Tech University, China, in 2001. Then he engaged in research at Fudan University, Kochi University, Tokyo University, Pennsylvania State University and University of Alabama during 2001–2010. Currently, he is a full professor at Nanjing Tech University. His research mainly focuses on the design, synthesis, and application of multifunctional materials (such as magnetic, optical electrical coupling materials and two-dimensional material).